Published in Applied Energy with doi: 10.1016/j.apenergy.2023.121062

An interval-based nested optimization framework for deriving flexibility from smart buildings and electric vehicle fleets in the TSO-DSO coordination

Seyed Amir Mansouri [1*], Emad Nematbakhsh[2], Ahmad Rezaee Jordehi [3], Mousa Marzband[1,4], Marcos Tostado-Véliz [5], Francisco Jurado [5]

[1] Northumbria University, Electrical Power and Control Systems Research Group, Ellison Place NE1 8ST, Newcastle upon Tyne, United Kingdom
[2] Faculty of Electrical Engineering, University of Isfahan, Isfahan, Iran
[3]Department of Electrical Engineering, Rasht Branch, Islamic Azad University, Rasht, Iran
[4] Center of Research Excellence in Renewable Energy and Power Systems, King Abdulaziz University, Jeddah 21589, Saudi Arabia
[5] Department of Electrical Engineering, University of Jaén, 23700, EPS Linares, Jaén, Spain

Abstract

Emerging renewable-based transmission and distribution systems, despite many environmental and economic benefits, due to the intermittent nature of their production resources, compared to traditional systems, need more flexibility capacities, which necessitates the need for more suppliers of flexibility. To deal with these challenges, a nested framework is presented to derive the required flexibility of the transmission system operator (TSO) from distributed energy resources (DERs) and active end-users such as smart buildings (SBs) and electric vehicle (EV) fleets at the distribution level. To this end, a novel mechanism to design the demand response program (DRP) is introduced in which tariffs with time-varying rewards are built based on flexibility requirements. The coordination between TSO and distribution system operator (DSO) is initially modeled as a bi-level non-linear programming (NLP) problem, in which the upper-level is day-ahead (DA) operational planning of DS considering the schedules received from SBs, while the lower-level is DA operational planning of the TS. The bi-level NIL problem is transformed into a single-level linear programming (LP) problem by Karush Kuhn Tucker (KKT) conditions, Big-M method and Strong Duality Theory (SDT), which makes it computationally tractable. Finally, a two-stage

* Corresponding Author: Amir.mansouri24@gmail.com

interval-based algorithm solves the obtained single-level problem to secure the planning against uncertainties where battery energy storage systems (BESSs) are responsible for dealing with extreme conditions. The simulation results testify that the proposed interval-based nested framework has improved the economic, technical and security aspects of the TSO-DSO coordination since it has reduced the daily costs of the energy and flexibility markets, relieved lines congestion and improved voltage characteristics.

Keywords: TSO-DSO Coordination; Energy and Flexibility Markets; Smart Buildings; Electric Vehicles; Strong Duality Theory, Demand Response Programs.

Nomenclature

Abbreviations	
BESS	Battery energy storage system
DA	Day-ahead
DER	Distributed energy resource
DG	Distribution generation
DRP	Demand response program
DS	Distribution System
DSO	Distribution system operator
EV	Electric vehicle
EWH	Electric water heater
FLMP	Flexibility locational marginal price
GT	Gas turbine
HVAC	Heating, ventilation and air conditioning
IGDT	Information gap decision theory
KKT	Krush Kuhn Tucker
LDC	Load demand curve
LMP	Locational marginal price
LP	Linear programming
NLP	Non-linear programming
PAR	Peak-to-average ratio
PV	Photovoltaic
RG	Renewable generation
RL	Regular load
SB	Smart building
SDT	Strong duality theory
SoC	State of charge
TS	Transmission system
TSO	Transmission system operator
TU	Thermal unit
V2G	Vehicle-to-grid
Sets	
b	SB index
dg	DG index
ds	Distribution-wide BESS index
ev	EV index
g	Transmission-wide generator index
i,j	Bus index of DSs
l	Line Index
n	Node index of TS
s	Transmission-wide BESS index

t	Time index
Scalar	
α^{AC}	HVAC thermal performance factor (C°/MWh)
α^{B}	Thermal constant of SB
Δt	Time step (h)
Δx	Insulation thickness (m)
η^{Ch} / η^{Dis}	Charge / Discharge efficiency of BESS/EV (%)
η^{PV}	Efficiency of PV panels (%)
G^{STD}	Standard sun irradiance (W/m2)
$\gamma^{Ch,\max} / \gamma^{Dis,\max}$	Max charge / discharge rate (%)
h	Heat transfer coefficient (W/m^{2}K)
k	Energy conversion constant (kWh/J)
κ^{B} / κ^{W}	Indoor / Water temperature discomfort rate
ω^{B} / ω^{W}	Indoor / Water temperature comfort weight
p	Specific heat of water (J/kgC°)
π^{Flex}	Flexibility reward coefficient ($/MW)
$SOC^{B,Initial}$	Initial SoC of BESS (%)
$SOC^{\min} / SOC^{\max}$	Min / Max SoC limit (%)
σ	Thermal conductivity (W/mK)
$\theta^{\min} / \theta^{\max}$	Min / Max voltage angle (rad)
θ^{Cold}	Cold water temperature (C°)
$\theta^{B,Initial} / \theta^{W,Initial}$	Initial value of water / indoor temperature (C°)
$V^{\min} / V^{\max}$	Min / Max voltage magnitude (p.u)
$v_{ci} / v_r / v_{co}$	Cut-in / Rated / Cut-out wind speed (m/s)
Parameters	
$\alpha_b^{DR-,\max} / \alpha_b^{DR+,\max}$	Max DRP rate for decreasing / increasing Demand (%)
$\alpha_{dg}^{\max}$	Reactive power rate of DG (%)
B_l / G_l	Susceptance / Conductance value of distribution line (p.u)
$\beta_{b,t}$	Flexibility signal
Cap_{ds}^{B}	BESS capacity (MWh)
Cap_{ev}^{EV}	EV's Battery capacity (MWh)
$Com_b^{Th,\min}$	Min comfort level (%)
$\Delta P_{b,t}^{Demand}$	Flexibility requirement (MW)
$E_s^{B,Initial}$	Initial energy of BESS (MWh)
$E_s^{\min} / E_s^{\max}$	Min/Max energy limit of BESS (MWh)
φ_i	Power factor of DS's buses
G_t	Sun irradiance (W/m^2)
$GSF_{l,i}$	Generation shift factor
$P_b^{AC,\max}$	Max power of HVAC (MW)
$P_s^{Ch,\max} / P_s^{Dis,\max}$	Max charge / discharge power (MW)
$\tilde{P}_{b,t}^{Building}$	Predicted demand of SBs (MW)
$P_{n,t}^{Demand}$	Active power demand of TS's nodes (MW)
$P_{b,t}^{DR-,\max} / P_{b,t}^{DR+,\max}$	Max DRP level for decreasing / increasing Demand (MW)

$P_b^{EWH,\max}$	Max power of EWH (MW)
$P_{dg}^{GT,\min}$ / $P_{dg}^{GT,\max}$	Min / Max power generation of GTs (MW)
$P_{i,t}^{Load}$ / $Q_{i,t}^{Load}$	Active / Reactive power demand of DS's buses (MW)
$P_{dg}^{PV,\max}$ / $P_g^{PV,\max}$	Max generation rate of PV farms (MW)
P_g^{RU} / P_g^{RD}	Ramp-up / Ramp-down limit of TUs (MW)
$P_g^{TU,\min}$ / $P_g^{TU,\max}$	Min / Max power generation of thermal units (MW)
$P_{dg}^{W,\max}$ / $P_g^{W,\max}$	Max generation rate of wind farms (MW)
π_{ds}^{B}	Operation cost of BESS ($/MWh)
$\pi_{ds}^{B,flex}$	Flexibility cost of BESS ($/MWh)
$\pi_{b,t}^{DR-}$ / $\pi_{b,t}^{DR+}$	DRP reward for decreasing / increasing demand ($/MWh)
π_t^{E}	Electricity price ($/MWh)
$\pi_t^{EV,Dch}$	V2G service reward ($/MWh)
π_{dg}^{DG}	Operation cost of DGs ($/MWh)
$\pi_{dg}^{GT,flex}$	Flexibility cost of GTs ($/MWh)
π_g^{TU}	Operation cost of TUs ($/MWh)
$\pi_g^{TU,flex}$	Flexibility cost of TUs ($/MWh)
R_l	Resistance value of DS's lines (p.u)
$SOC_{ev}^{EV,Initial}$ / $SOC_{ev}^{EV,Final}$	Initial / Final SoC rate of EV's battery (%)
$S_l^{Line,\max}$	Max apparent power of lines (MVA)
$S_b^{surface}$	Total surface area (m^2)
T_b^{a} / T_b^{d}	Arrival / Departure Time (h)
θ_t^{Amb}	Ambient temperature (C°)
$\theta_t^{B,\min}$ / $\theta_t^{B,\max}$	Min / Max indoor temperature (C°)
$\theta_{b,t}^{B,Des}$ / $\theta_{b,t}^{W,Des}$	Desired indoor / water temperature (C°)
$\theta_t^{W,\min}$ / $\theta_t^{W,\max}$	Min / Max water temperature (C°)
v_t	Hourly wind speed (m/s)
$v_{b,t}^{tank}$	Volume of the stored water in tank (kg)
$\xi_{l,i}$	Flow direction factor

Variables

Com_b^{Th}	Comfort index (%)
$\Delta P_{b,t}^{AC}$	Changes in HVAC operation points before and after DRP (MW)
$\Delta P_{b,t}^{B,Ch}$ / $\Delta P_{b,t}^{B,Dis}$	Changes in charge / discharge value of BESS before and after DRP (MW)
$\Delta P_{ds,t}^{B,up}$ / $\Delta P_{ds,t}^{B,Down}$	Upward / Downward flexibility participation rate of distribution-wide BESS (MW)
$\Delta P_{s,t}^{B,up}$ / $\Delta P_{s,t}^{B,Down}$	Upward / Downward flexibility participation rate of distribution-wide BESS (MW)
$\Delta P_{ev,t}^{EV,Ch}$ / $\Delta P_{ev,t}^{EV,Dis}$	Changes in charge / discharge value of EV's battery before and after DRP (MW)
$\Delta P_{b,t}^{EWH}$	Changes in EWH operation points before and after DRP (MW)

$\Delta P_{dg,t}^{GT,up}$ / $\Delta P_{dg,t}^{GT,down}$	Upward / Downward flexibility participation rate of GTs (MW)
$\Delta P_{g,t}^{TU,up}$ / $\Delta P_{g,t}^{TU,down}$	Upward / Downward flexibility participation rate of TUs (MW)
$E_{s,t}^{B}$	Energy level of BESS (MWh)
$P_{b,t}^{AC}$	HVAC power usage (MW)
$P_{ds,t}^{B,Ch}$ / $P_{ds,t}^{B,Dis}$	Charged / Discharged power in / from BESS (MW)
$P_{s,t}^{B,Ch}$ / $P_{s,t}^{B,Dis}$	Charged / Discharged power in / from BESS (MW)
$P_{b,t}^{Building}$	Power usage of SB (MW)
$P_{dg,t}^{DG}$	Generated power by DGs (MW)
$P_{ev,t}^{EV,Ch}$ / $P_{ev,t}^{EV,Dis}$	Charged / Discharged power in / from EV's battery (MW)
$P_{b,t}^{EWH}$	EWH power usage (MW)
$P_{g,t}^{G}$	Generated power by transmission-wide generator (MW)
$P_{dg,t}^{GT}$	Generated power by GTs (MW)
$P_{l,t}^{Line}$ / $Q_{l,t}^{Line}$	Active / Reactive power flow (MW/MVAR)
$P_{l,t}^{Loss}$	Active power loss (MW)
$P_{b,t}^{Net}$	Net load of SB (MW)
$P_{d,t}^{PCC}$ / $Q_{d,t}^{PCC}$	Active / Reactive power exchange in coupling nodes (MW/MVAR)
$P_{d,t}^{PCC,up}$ / $P_{d,t}^{PCC,down}$	Upward / downward flexibility exchange in coupling nodes (MW)
$P_{dg,t}^{PV}$ / $P_{g,t}^{PV}$	Generated power by PV farms (MW)
$P_{g,t}^{TU}$	Generated power by TUs (MW)
$P_{dg,t}^{W}$ / $P_{g,t}^{W}$	Generated power by wind farms (MW)
$\pi_{d,t}^{LMP}$	LMP at coupling point ($/MWh)
$\pi_{n,t}^{FLMP}$	FLMP at coupling point ($/MWh)
$Q_{b,t}^{EWH}$	Energy demand of EWH (kWh)
$Q_{b,t}^{Loss}$	Energy losses in EWH's tank (kWh)
$SOC_{ds,t}^{B}$	SoC of BESS (%)
$SOC_{ev,t}^{EV}$	SoC of EV's battery (%)
$\theta_{i,t}$	Voltage angle (rad)
$\theta_{b,t}^{B}$	Indoor temperature (C^{o})
$\theta_{b,t}^{W}$	Water temperature (C^{o})
$V_{i,t}$	Voltage magnitude (p.u)

Binary Variables

$I_{ds,t}^{B,Ch}$ / $I_{ds,t}^{B,Dis}$	Charge / Discharge status of BESS
$I_{c,t}^{DR-}$ / $I_{c,t}^{DR+}$	Downward / Upward status of DRP
$I_{ev,t}^{EV,Ch}$ / $I_{ev,t}^{EV,Dis}$	Charge / Discharge status of EV

1. Introduction

1.1. Background and Motivation

Climate changes caused by global warming in recent years have made it inevitable to replace fossil fuel production sources with renewable technologies (RGs) in the electrical and transportation sectors, since these sectors have the largest share of carbon emissions [1]. This technology change is called energy transition, which despite the many environmental advantages, brings some technical challenges due to the intermittent nature of RGs. On the other hand, the replacement of fossil fuel vehicles with electric ones will make the future transport fleet directly dependent on the electric sector, which creates new technical and security challenges for electricity grids [2]. It is noteworthy to state that EVs are like mobile loads that are moved throughout the network and the exact time of their connection to the network is unpredictable [3]. In general, the increase in the number of sources with stochastic behavior such as RGs and EVs in emerging renewable-based electrical networks threatens the stability and security of their operation. Therefore, threats caused by increasing uncertainties are one of the main challenges of renewable-based networks, which necessitates the expansion of ancillary services such as flexibility services to overcome stability and security threats [4].

In emerging renewable-based electricity networks, providing system flexibility is one of the serious challenges of operators since it has a large number of renewable resources whose operating point is unadjustable. Therefore, operators of emerging renewable-based electricity networks must provide their required flexibility through new sources, since the share of fossil fuel production units in these networks will be low [5]. In this regard, purchasing local flexibility services is an effective and affordable solution [6]. Smart end-users, distributed generations (DGs) and BESSs within distribution systems are three important sources for providing local flexibility services. For example, SBs equipped with thermostatic loads such as heating, ventilation and air conditioning (HVAC) and electric water heater (EWH) systems can make a significant contribution to meeting the flexibility needs of the system by changing the operating point of these systems [7,8].

DRPs are necessary to extract maximum flexibility capacities from smart end-users [9]. These programs are a key solution to motivate smart end-users to meet part of the system's flexibility needs. DRPs can mitigate the mismatch between production and consumption in the system by providing incentive tariffs in normal and emergency conditions [10]. It should be noted that the implementation of time-varying DRPs requires smart meters and a reliable connection between end-users and operators [11]. One of the important challenges that must be addressed to ensure the stability of emerging renewable-based networks is how to design DRPs in line with system flexibility requirements, which is specifically addressed in this article.

1.2. Literature Review

The increase in uncertainties caused by the high-penetration of RGs and EVs in power systems has increased the need for ancillary services since these services greatly increase the safety and reliability of network operation. Some studies have shown that distribution-wide DERs can meet a significant share of system flexibility needs [12]. For example, the authors of [13] presented an optimal strategy for the participation of DSs in the energy and reserve markets, taking into account the uncertainties caused by RGs. This strategy is first modeled as two-stage problem where DS operation is done in stage 1 while TS operation is done in stage 2. Then, the two-stage strategy is transformed into a single-stage LP problem by KKT and SDT conditions and solved. The results demonstrate that distribution-wide DERs have significantly reduced daily costs through active participation in energy and reserve markets. The studies done in [14] show that the increase of RGs leads to congestion in the network unless the infrastructure is developed or new flexible resources are introduced. The authors of [15] have introduced a new market-based strategy through which TSO can provide a large part of the required flexibility through distribution-wide DERs. The objective function of this strategy is to minimize the operating costs imposed by DSOs on DERs. The proposed model is implemented on a DS located in Great Britain and in that scenario, the increase in the number of DERs until 2030 is considered. The simulation results reflect that the proposed strategy gives the priority of providing flexibility services to the DERs located in the DS. [16] proposes a

new strategy to estimate the flexibility capacities of DERs in different areas of the DS. The authors of this research presented a methodology called Grid Structure Optimization, in which different system flexibility areas are divided into two categories, low and medium speed response, based on their response speed. This methodology has been implemented on both 9- and 13-node networks and the results confirm its effectiveness in supplying flexibility capacities from DERs and also in reducing the flexibility locational marginal price (FLMP). Furthermore, the analysis of the results proves that the flexibility of DERs is necessary to control the frequency of the system under emergency situations. In [17], the significant effects of optimal control of active power on improving the security indicators of electrical networks have been shown.

The technical, economic, environmental and security effects of the EV fleets on the operation of electric networks is one of the most important issues that should always be considered in short-term and long-term planning [18,19]. The authors in [20] presented an optimal structure for the intelligent scheduling of the transportation system and electric vehicles based on the exchange of information between them, which leads to the improvement of the technical and security indicators of the system. In [21], the great importance of communication between the EV fleets and the central control system of the transportation network on improving the efficiency of the system has been confirmed.

Accurate modeling of uncertainties in the operational planning of emerging renewable-based power systems is essential for their reliable, safe and cost-effective operation [22]. In this regard, the authors of [23] presented a two-stage decentralized structure for the simultaneous management of wholesale and retail markets in the TSO-DSO interface under the influence of a large number of RGs, in which an information gap decision theory (IGDT)-based strategy is used to model the uncertainties of RGs output and load demand. The first and second stages settle the wholesale and retail markets, respectively. The simulation results prove the impact of the proposed methodology on the more optimal use of RGs capacity and subsequently on reducing locational marginal price (LMP). [24] presented a new strategy for aggregating flexibility from distribution-wide DERs to meet TSO flexibility requirements, in which a risk-

averse method was used to overcome operational uncertainties. In the introduced strategy, the errors related to the forecasting of load and production of RGs, as well as contingent events are considered. This strategy has been implemented on a coordinated TSO-DSO in Switzerland and the results confirm its eligibility. In [25], a comprehensive structure for congestion management in transmission systems under the influence of RGs is presented, in which chance-constrained technique is adopted to cope with uncertainties arising from load demand and production of wind farms. Chance constraints are applied on the network power flow equations to cover mismatches between production and consumption. The results testify that the proposed structure has reduced the density of sensitive lines under normal operation conditions, while under emergency situations, it has reduced load shedding by considering higher spinning reservation.

Some researchers have shown that DRPs are an excellent solution to modify the consumption pattern of smart end-users and extract flexibility from them [26,27]. For instance, the authors of [28] have presented a cloud-based structure to facilitate the implementation of DRPs in SBs within a local grid. The results of this research show that the proposed structure modifies the consumption pattern of SBs by changing the operation time of controllable appliances and subsequently unlocks their flexibility capacity. In [29], the authors presented a multi-level strategy to enable demand-side flexibility by proposing DRPs to SBs, in which the available flexibility capacity of SBs is estimated for the day-ahead operational planning. In this research, the scheduling of thermostatic loads, BESSs and EVs was done in both normal and flexible conditions in order to estimate their flexible potential. The simulation results substantiate the impact of the proposed DRP-based strategy on reducing the daily operating costs of the TN. In [30], the authors have investigated the impact of DRPs and BESSs on the technical and economic indicators of distribution systems. In this regard, different DRPs have been implemented on residential, industrial and commercial energy hubs, and the results show that the participation of hubs in these programs has led to the release of a lot of flexibility in peak periods. In addition, the results show that the installation of BESSs in hubs greatly increases their potential for the flexibility provision. The authors in [31] have shown that

thermostatic loads such as HVAC, EWH, heat pump (HP), etc. have a significant potential to participate in DRPs and subsequently provide flexibility to the network. These authors present a new strategy for quantifying thermostatic loads within the network. Also, a new control method is presented to overcome the synchronization problem of thermostatic loads, since this problem can affect their available flexibility. The results reflect that this strategy has been able to minimize the power and frequency fluctuations of the network by using DRPs. [32] presents a new structure for the precise design of incentive-based DRPs, where the rewards paid to subscribers are determined based on their behavior and electricity price elasticity. The proposed structure has been used to manage the energy consumption pattern of microgrids within the DS and the results confirm that this structure has been able to enhance the economic and technical factors of the operation.

Several studies have also evaluated the effects of dynamic thermal rating on the technical, security and economic aspects of power systems. The dynamic thermal rating is a safe system for determining thermal limits of network equipment according to environmental conditions. In [33], a comprehensive review on the applications of dynamic thermal rating in TSs, DSs and transformers has been done. In this research, the background and current state-of-art of dynamic thermal rating systems have been accurately evaluated. In [34], the authors have shown that network topology optimization by considering dynamic thermal rating system and BESSs reduces daily system costs, network congestion and renewable power curtailment. Similarly, it has been shown in [35] that the simultaneous consideration of dynamic thermal rating system and BESSs not only increases the operational reliability but also reduces network losses and congestion. In [36], the authors declare that power systems with the simultaneous presence of dynamic thermal rating system and DRP require smaller BESSs, which will lead to a significant reduction in system planning costs.

1.3. Research Gap and Contribution

The literature review clarifies that most researchers have used DRPs to modify the load demand curve (LDC) to achieve goals such as reducing operating costs, increasing reliability, minimizing peak-to-

average ratio (PAR), etc., and there is a large gap in the field of designing time-varying DRPs with the aim of adapting the behavior of smart end-users with flexibility requirements of renewable-based electricity networks. Also, the review of the past literature indicates that there is a big gap in the studies of the impact of the behavior of SBs and EV fleets on the coordination between TSO and DSO, as well as their potential to meet system flexibility requirements. Therefore, the authors of this article design a nested framework to develop the coordination between TSO and DSO in energy and flexibility markets, in which a new mechanism for designing time-varying DRPs based on system flexibility requirements is embedded. In this article, we examine in detail the effects of the behavior of SBs and EV fleets on the technical, economic and security metrics of the system, including market costs, voltage profile and network congestion. Below are the main innovations of this article:

- Presenting a nested framework to coordinate TSO and DSO in energy and flexibility markets in which SBs are scheduled considering occupants' thermal comfort in a decentralized space with minimal data sharing.
- Presenting a novel DRP design mechanism to build time-varying incentive tariffs based on TSO's flexibility requirements to drive flexibility capacities from smart buildings and EV fleets.
- Improving operational security by developing a two-stage interval-based optimization method to deal with uncertainties arising from the output of RGs and load demand where BESSs guarantee safe operation in extreme conditions.
- Using KKT conditions, SDT and Big-M method to convert the bi-level NLP problem of the TSO-DSO coordination into a convergent single-level LP problem which makes the proposed framework computationally tractable.
- Providing a considerable part of the system's required flexibility through distribution-wide sources including GTs, BESSs, SBs and EV fleets, which in addition to the significant reduction of LMP and FLMP at the coupling nodes, leads to a reduction in congestion and improvement of voltage profile in both transmission and distribution networks.

2. Model Outline and Problem Formulation

In this paper, we have presented a nested framework to optimize the DA interactions of energy and flexibility markets in the TSO-DSO interface by exploiting the potential of SBs and EV fleets, as its architecture is shown in Fig. 1. As per this architecture, the proposed framework is initially modeled as a bi-level problem whose upper level consists of three layers. In layer 1, DSOs find the DA flexibility requirements from the TSO to design DRP tariffs with time-varying incentives based on them. At the end of this layer, DSOs send the designed tariff to SBs so that the SBs can do their DA scheduling according to them. In layer 2, optimal DA scheduling of SBs is conducted in a decentralized space by their energy management system (EMS). In this layer, each SB plans thermostatic loads including HVAC and EWH, BESS and charging/discharging of EVs according to the incentive tariffs received from DSO and then sends its final plan including shortage/surplus of DA hourly demand to DSO. At the end of layer 2, the load demand of DS nodes is updated according to the programs received from SBs. Afterward, in layer 3, operational planning of DS is done with the aim of minimizing DA costs, taking into account energy and flexibility markets. In this layer, distribution-wide GTs and BESSs participate in the flexibility market.

Operational planning of TS is done at the lower-level. Since the electricity prices at the coupling points between TS and DSs are variable, the optimization problem of the third layer of upper-level (Operational planning of DS) becomes an NLP problem that makes the bi-level model non-convergent. Therefore, the third layer of the upper-level (Operational planning of DS) and the lower-level are integrated using KKT conditions, Big-M method and SDT to form a convergent single-level LP problem. According to the architecture, it can be seen that in the last step, a two-stage interval-based optimization algorithm is used to solve the built single-level problem. In this algorithm, the values of all planning variables are determined according to the fluctuations of uncertain parameters, where BESSs guarantee safe operation in extreme conditions.

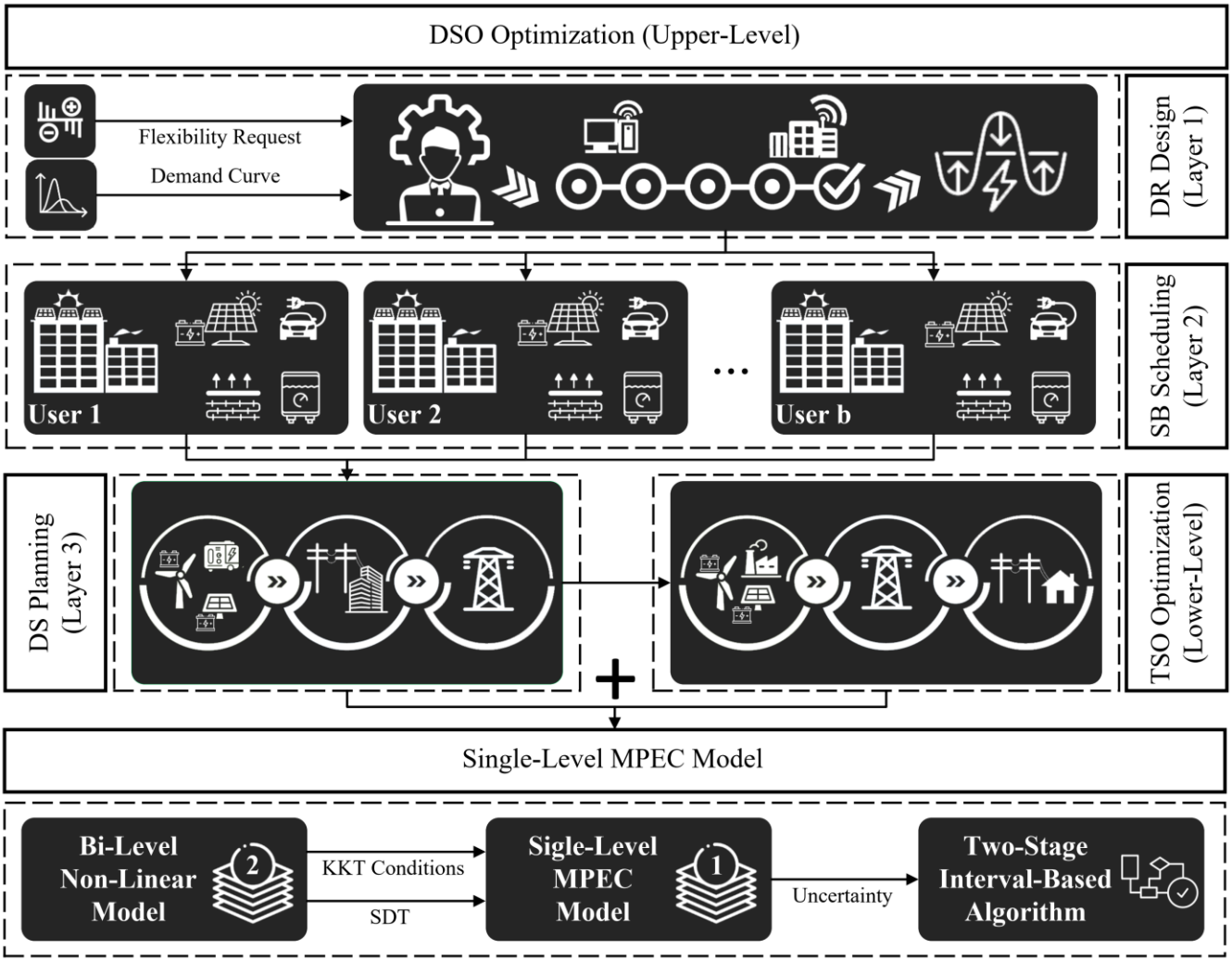

Fig. 1. The architecture of the proposed nested framework

Each part of the mathematical modeling of the proposed nested framework is introduced in a separate subsection below.

2.1 Upper-Level (DSO Optimization)

2.1.1. Layer 1 (DRP Design Mechanism)

The functions presented in Eqs. (1) and (2) model the layer 1 of upper-level where DRP tariffs are constructed by the DSO according the flexibility requirements of the TSO. The rewards of these tariffs are time-varying. $\Delta P_{b,t}^{Demand}$ is the flexibility required by TSO at time t; $\Delta P_{b,t}^{Demand} \geq 0$ refers to upward flexibility capacity while $\Delta P_{b,t}^{Demand} \leq 0$ refers to downward flexibility capacity. These functions state that

when TSO requests upward flexibility, DSO designs DRP tariffs with the aim of motivating SBs to reduce their load demand, while when downward flexibility capacity is requested, tariffs are designed with the aim of increasing SBs' load demand. $P_{b,t}^{DR+,\max}$ and $P_{b,t}^{DR-,\max}$ are respectively the maximum levels of load increment and load decrement, which are limited to a percentage ($\alpha_b^{DR-,\max}$ / $\alpha_b^{DR+,\max}$) of the load of SBs. $\tilde{P}_{b,t}^{Building}$ is the average load demand of the last ten days of SB b at time t. $\pi_{b,t}^{DR+}$ and $\pi_{b,t}^{DR-}$ refer to load increment and load decrement rewards which are calculated by exponential functions according to the upward and downward flexibility requirements. According to these exponential functions, the higher the demand for flexible capacities, the higher the reward. $\beta_{b,t}$ is a binary variable that prevents bonus payments in hours when flexibility demands are zero.

$$\Delta P_{b,t}^{Demand} \geq 0 \Rightarrow \begin{cases} P_{b,t}^{DR-,\max} = \alpha_b^{DR-,\max} \tilde{P}_{b,t}^{Building} \\ \pi_{b,t}^{DR-} = \pi^{Flex} \beta_{b,t} e^{\kappa^{DR-} \frac{\Delta P_{b,t}^{Demand}}{\max_t \left(\Delta P_{b,t}^{Demand} \right)}} \\ \beta_{b,t} = \begin{cases} 0 & , \ \Delta P_{b,t}^{Demand} = 0 \\ 1 & , \ otherwise \end{cases} \end{cases} \tag{1}$$

$$\Delta P_{b,t}^{Demand} \leq 0 \Rightarrow \begin{cases} P_{b,t}^{DR+,\max} = \alpha_b^{DR+,\max} \tilde{P}_{b,t}^{Building} \\ \pi_{b,t}^{DR+} = \pi^{Flex} \beta_{b,t} e^{\kappa^{DR+} \frac{\left| \Delta P_{b,t}^{Demand} \right|}{\max_t \left(-\Delta P_{b,t}^{Demand} \right)}} \\ \beta_{b,t} = \begin{cases} 0 & , \ \Delta P_{b,t}^{Demand} = 0 \\ 1 & , \ otherwise \end{cases} \end{cases} \tag{2}$$

2.1.2. Layer 2 (Scheduling of SBs)

Layer 2 of the upper-level is formulated in this subsection. The objective function of SBs' scheduling is introduced in Eq. (3), while its operating constraints are modeled by (a1)-(b7). As per Eq. (3), the aim of the SBs' EMS is to minimize DA costs. Equation 3 reveals that the costs of SB consist of the cost of purchasing power and the cost of BESS operation. This equation also expresses that the SB can earn profit through providing V2G services and participating in DRP.

$$OF_b^{Layer2} = \min \sum_t \left(\pi_t^E P_{b,t}^{Net}\right)\Delta t + \sum_t \sum_{ds\in\Delta_b^{ds}} \pi_{ds}^B \left(P_{ds,t}^{B,Ch} + P_{ds,t}^{B,Dis}\right) - \sum_t \sum_{ev\in\Delta_b^{ev}} \left(\pi_t^{EV,Dch} P_{ev,t}^{EV,Dis}\right)\Delta t - \sum_t \left(P_{b,t}^{DR+}\pi_{b,t}^{DR+} + P_{b,t}^{DR-}\pi_{b,t}^{DR-}\right)\Delta t \quad (3)$$

- **Smart Building**

In (a1) to (a20) SBs are modeled. These buildings have rooftop solar panel (RSP), BESS, HVAC, EWH and EV parking. Equation (a1) calculates the net load demand of each SB [29]. As per this equation, the power produced by RSP has been deducted from the load. The load demand curve of the SB after participating in DRP ($P_{b,t}^{Building}$) is determined in Eq. (a2). $\tilde{P}_{b,t}^{Building}$ refers to the demand curve of the SB before participating in DRP, whereas $P_{b,t}^{DR+}$ and $P_{b,t}^{DR-}$, respectively, refer to the load increase and decrease after participating in DRP. According to Eq. (a3), HVAC, EWH, BESS and EVs are participants in DRP. Equation (a4) calculates the changes in the operating points of the mentioned devices. $\tilde{P}^X$ represents the operating point of the component before participating in DRP, while P^X represents its operating point after participating in DRP. Equations (a5) and (a6) are introduced to prevent over-participation in DRP. Eq. (a7) manages the non-simultaneity of load increase and decrease.

Equation (a8) determines the water temperature ($\theta_{b,t}^W$) of the EWH tank at time *t*. $P_{b,t}^{EWH}$ and $Q_{b,t}^{Loss}$ refer to the power consumption and energy losses of the EWH tank, respectively; $Q_{b,t}^{EWH}$ is the thermal energy required to heat the incoming cold water to the EWH tank; $v_{b,t}^{tank}$ is the volume of water consumed, whereas k and p are respectively the energy and heat conversion constants of water. $\theta_{b,t-1}^W$ refers to the tank water temperature in the previous hour. Condition (a9) sets the tank water temperature at a fixed value at the start of operation. Condition (a10) confines the tank water temperature changes to a predetermined region. Equation (a11) determines the thermal energy required to heat the incoming cold water (θ^{Cold}). Equation (a12) guarantees the supply of electrical energy needed to heat the incoming water. Condition (a13) confines electricity consumption of EWH. Equation (a14) calculates the heat losses of the tank based on the difference between the tank water temperature ($\theta_{b,t}^W$) and the ambient temperature (θ_t^{Amb}) [37]. The

amount of tank losses also depends on the area of the contact surface of the tank with the outside air ($S_{surface}$), as well as the insulation thickness (Δx), heat transfer coefficient (h) and thermal conductivity (σ).

The indoor temperature ($\theta_{b,t}^{B}$) of the SB is calculated by Eq. (a15), which is a function of the indoor temperature the SB in the previous hour ($\theta_{b,t-1}^{B}$), the ambient temperature in the current hour (θ_{t}^{Amb}), and the power consumption of the HVAC system ($P_{b,t}^{AC}$) [38]. By condition (a16), the indoor temperature of the SB is set to a constant value at the start of operation. Condition (a17) shows the permissible range of changes in the indoor temperature of the building. Condition (a18) confines the power consumption of HVAC. Ultimately, the thermal comfort index of the SB is obtained via Eq. (a19) whereas it is limited by (a20). Note that the operation of BESSs of SBs is based on Eqs. (d1)-(d6) while the operation of RSPs is according to the Eq. (c1).

$$P_{b,t}^{Net} = P_{b,t}^{Building} - \sum_{dg \in \Omega_b^{dg}} P_{dg,t}^{PV} \tag{a1}$$

$$P_{b,t}^{Building} = \tilde{P}_{b,t}^{Building} + P_{b,t}^{DR+} - P_{b,t}^{DR-} \tag{a2}$$

$$P_{b,t}^{DR+} - P_{b,t}^{DR-} = \Delta P_{b,t}^{AC} + \Delta P_{b,t}^{EWH} + \Delta P_{b,t}^{B,Ch} - \Delta P_{b,t}^{B,Dis} + \sum_{ev \in \Omega_b^{ev}} \left(\Delta P_{ev,t}^{EV,Ch} - \Delta P_{ev,t}^{EV,Dis} \right) \tag{a3}$$

$$\Delta P^{X} = P^{X} - \tilde{P}^{X} \quad , \quad X \in \left\{ P_{b,t}^{AC}, P_{b,t}^{EWH}, P_{b,t}^{B,Ch}, P_{b,t}^{B,Dis}, P_{ev,t}^{EV,Ch}, P_{ev,t}^{EV,Dis} \right\} \tag{a4}$$

$$0 \le P_{b,t}^{DR+} \le P_{b,t}^{DR+,\max} I_{b,t}^{DR+} \tag{a5}$$

$$0 \le P_{b,t}^{DR-} \le P_{b,t}^{DR-,\max} I_{c,t}^{DR-} \tag{a6}$$

$$0 \le I_{b,t}^{DR+} + I_{b,t}^{DR-} \le 1 \tag{a7}$$

$$\theta_{b,t}^{W} = \theta_{b,t-1}^{W} + \frac{P_{b,t}^{EWH} \Delta t - Q_{b,t}^{EWH} - Q_{b,t}^{Loss}}{kpv_{b,t}^{tank}} \tag{a8}$$

$$\theta_{b,t=0}^{W} = \theta^{W,Initial} \tag{a9}$$

$$\theta_{t}^{W,\min} \le \theta_{b,t}^{W} \le \theta_{t}^{W,\max} \tag{a10}$$

$$Q_{b,t}^{EWH} = kpv_{b,t}^{tank} \left(\theta_{b,t}^{W} - \theta^{Cold} \right) \tag{a11}$$

$$P_{b,t}^{EWH} \Delta t \ge Q_{b,t}^{EWH} \tag{a12}$$

$$0 \le P_{b,t}^{EWH} \le P_{b}^{EWH,\max} \tag{a13}$$

$$Q_{b,t}^{Loss} = \frac{\theta_{b,t}^{W} - \theta_{t}^{Amb}}{\frac{\Delta x}{\sigma} + \frac{1}{h}} S_{b}^{surface} \tag{a14}$$

$$\theta_{b,t}^{B} = \left(1-\alpha^{B}\right)\theta_{b,t-1}^{B} + \alpha^{B}\theta_{t}^{Amb} + \alpha^{AC}P_{b,t}^{AC}\Delta t \quad \text{(a15)}$$

$$\theta_{b,t=0}^{B} = \theta^{B,Initial} \quad \text{(a16)}$$

$$\theta_{t}^{B,\min} \le \theta_{b,t}^{B} \le \theta_{t}^{B,\max} \quad \text{(a17)}$$

$$0 \le P_{b,t}^{AC} \le P_{b}^{AC,\max} \quad \text{(a18)}$$

$$Com_{b}^{Th} = \left(\omega^{W} \sum_{t} \frac{e^{-\kappa^{W}\left|\theta_{b,t}^{W}-\theta_{b,t}^{W,Des}\right|}}{24} + \omega^{B} \sum_{t} \frac{e^{-\kappa^{B}\left|\theta_{b,t}^{B}-\theta_{b,t}^{B,Des}\right|}}{24} \right) \times 100 \quad \text{(a19)}$$

$$Com_{b}^{Th} \ge Com_{b}^{Th,\min} \quad \text{(a20)}$$

- **EV fleets**

EV fleets are included in the model by Eqs. (b1)-(b8). In this regard, Eq. (b1) reveal that the hourly charge ($P_{ev,t}^{EV,Ch}$) and discharge ($P_{ev,t}^{EV,Dis}$) of the EV battery should be within a limited range. $I_{ev,t}^{EV,Ch}$ and $I_{ev,t}^{EV,Dis}$ are respectively decision variables that determine charging and discharging states of the EV battery. Equation (b2) states that the operation of EVs is possible only if they are present in the parking lots. Condition (b3) does not allow simultaneous charging and discharging the EV. Equation (b4) determines the SoC of the EV battery at time *t*, while Eqs. (b5) and (b6) determine the SoC of EVs at the entry and exit times to/from the parking lot, respectively. It is noteworthy to state that the SoC of the EV battery at the time of entering the parking lot ($SOC_{ev}^{EV,Initial}$) is a random parameter between 0.35 and 0.5, which is obtained through the uniform probability distribution function. Besides, the SoC of the EV battery at the time of leaving the parking lot ($SOC_{ev}^{EV,Final}$) is considered equal to 95% of its capacity. Condition (b7) confines the SoC of the EV battery during the scheduling period.

$$\begin{cases} 0 \le P_{ev,t}^{EV,Ch} \le \gamma^{Ch,\max} Cap_{ev}^{EV} I_{ev,t}^{EV,Ch} \\ 0 \le P_{ev,t}^{EV,Dis} \le \gamma^{Dis,\max} Cap_{ev}^{EV} I_{ev,t}^{EV,Dis} \end{cases} \quad \forall ev, \forall t \in [T_b^a, T_b^d) \quad \text{(b1)}$$

$$\begin{cases} P_{ev,t}^{EV,Ch} = 0 \\ P_{ev,t}^{EV,Dis} = 0 \end{cases} \quad \forall ev, \forall t \notin [T_b^a, T_b^d) \quad \text{(b2)}$$

$$0 \le I_{ev,t}^{EV,Ch} + I_{ev,t}^{EV,Dis} \le 1 \quad \text{(b3)}$$

$$SOC_{ev,t}^{EV} = SOC_{ev,t-1}^{EV} + \frac{\eta^{Ch} P_{ev,t}^{EV,Ch} - \frac{P_{ev,t}^{EV,Dis}}{\eta^{Dis}}}{Cap_{ev}^{EV}} \Delta t \quad \text{(b4)}$$

$$SOC_{ev,t=T^a}^{EV} = SOC_{ev}^{EV,Initial} \quad \text{(b5)}$$

$$SOC_{ev,t=T^d}^{EV} = SOC_{ev}^{EV,Final} \tag{b6}$$

$$SOC^{\min} \le SOC_{ev,t}^{EV} \le SOC^{\max} \tag{b7}$$

2.1.3. Layer 3 (Operational Planning of DSO)

In this subsection, layer 3 of the upper-level is modeled, where Eq. (4) provides the DSO objective function and Eqs. (c1)-(e9) provide its operation constraints. As per Eq. (4), the goal of DSO is to minimize the DA costs of its service area. The first and second terms of Eq. (4) respectively model the costs of purchasing power from DGs and BESSs, taking into account their participation in the energy and flexibility markets. The third term of Eq. (4) denotes the cost of purchasing power from TSO, where $P_{d,t}^{PCC}$ and $\pi_{d,t}^{LMP}$ refer to the power purchased from TSO and electricity price at coupling node, respectively. Lastly, the fourth term of Eq. (4) denotes the profit of selling upward and downward flexibility services to TSO.

$$OF^{Layer3} = \min \sum_{d} \sum_{t} \left[\begin{array}{l} \sum_{dg \in \Delta_d^{dg}} \left[\pi_{dg}^{DG} P_{dg,t}^{DG} + \pi_{dg}^{GT,\,flex} \left(\Delta P_{dg,t}^{GT,up} + \Delta P_{dg,t}^{GT,down} \right) \right] \\ + \sum_{ds \in \Delta_d^{ds}} \left[\pi_{ds}^{B} \left(P_{ds,t}^{B,Ch} + P_{ds,t}^{B,Dis} \right) + \pi_{ds}^{B,\,flex} \left(\Delta P_{ds,t}^{B,up} + \Delta P_{ds,t}^{B,down} \right) \right] \\ + \pi_{d,t}^{LMP} P_{d,t}^{PCC} - \left(\pi_{d,t}^{FLMP,up} P_{d,t}^{PCC,up} + \pi_{d,t}^{FLMP,down} P_{d,t}^{PCC,down} \right) \end{array} \right] \tag{4}$$

- **Distributed Energy Resources**

Equations (c1)-(c4) formulate distribution-wide DGs consisting of wind turbines, centralized PV farms and gas turbines (GTs). In this way, Eq. (c1) determines the generation rate of wind farms according to the hourly wind speed (v_t). Equation (c2) states that the power extracted from centralized PV farms depends on its capacity ($P_{dg}^{PV,\max}$), the radiation at time t (G_t) and inverter efficiency (η^{PV}). Active and reactive powers produced by GTs are respectively confined by (c3) and (c4). $P_{dg,t}^{GT}$ is the capacity assigned to the energy market, while $\Delta P_{dg,t,sc}^{GT,up}$ and $\Delta P_{dg,t,sc}^{GT,down}$ are respectively the capacities assigned to the upward and downward flexibility markets.

$$P_{dg,t}^{W}=\begin{cases}0 & ,\ v_t<v_{ci}\quad \text{Or}\ \ v_t\geq v_{co}\\ P_{dg}^{W,\max}\left(\dfrac{v_t^2-v_{ci}^2}{v_r^2-v_{ci}^2}\right) & ,\ v_{ci}\leq v_t<v_r\\ P_{dg}^{W,\max} & ,\ v_r\leq v_t<v_{co}\end{cases} \tag{c1}$$

$$P_{dg,t}^{PV}=\eta^{PV}\frac{G_t}{G^{STD}}P_{dg}^{PV,\max} \tag{c2}$$

$$P_{dg}^{GT,\min}\leq P_{dg,t}^{GT}+\Delta P_{dg,t,sc}^{GT,up}-\Delta P_{dg,t,sc}^{GT,down}\leq P_{dg}^{GT,\max} \tag{c3}$$

$$-\alpha_{dg}^{\max}\left(P_{dg,t}^{GT}+\Delta P_{dg,t,sc}^{GT,up}-\Delta P_{dg,t,sc}^{GT,down}\right)\leq Q_{dg,t}^{GT}\leq\alpha_{dg}^{\max}\left(P_{dg,t}^{GT}+\Delta P_{dg,t,sc}^{GT,up}-\Delta P_{dg,t,sc}^{GT,down}\right) \tag{c4}$$

- **Distribution-Wide Battery Energy Storage Systems**

The operating constraints of distribution-wide BESSs are formulated in (d1)-(d6). Condition (d1) limits that the sum of the discharged power ($P_{ds,t}^{B,Dis}$) and the capacity allocated to the upward flexibility market by the BESS ($\Delta P_{ds,t}^{B,up}$) per hour. Condition (d2) similarly confines the sum of the charged power ($P_{ds,t}^{B,Ch}$) and the capacity allocated to the downward flexibility market by the BESS ($\Delta P_{ds,t}^{B,down}$) per hour. Condition (d3) does not allow simultaneous activation of charge ($I_{ds,t}^{B,Ch}$) and discharge ($I_{ds,t}^{B,Dis}$) decision variables. Equation (d4) calculates SoC of the BESS in each hour of operation while Eq. (d5) sets the SoC at both start and end times of operation on the $SOC^{B,Initial}$ parameter. Up and down levels of the SoC are restricted in (d6).

$$0\leq P_{ds,t}^{B,Dis}+\Delta P_{ds,t}^{B,up}\leq\gamma^{Dis,\max}Cap_{ds}^{B}I_{ds,t}^{B,Dis} \tag{d1}$$

$$0\leq P_{ds,t}^{B,Ch}+\Delta P_{ds,t}^{B,down}\leq\gamma^{Ch,\max}Cap_{ds}^{B}I_{ds,t}^{B,Ch} \tag{d2}$$

$$0\leq I_{ds,t}^{B,Dis}+I_{ds,t}^{B,Ch}\leq 1 \tag{d3}$$

$$SOC_{ds,t}^{B}=SOC_{ds,t-1}^{B}+\frac{\eta^{Ch}\left(P_{ds,t}^{B,Ch}+\Delta P_{ds,t}^{B,down}\right)-\dfrac{\left(P_{ds,t}^{B,Dis}+\Delta P_{ds,t}^{B,up}\right)}{\eta^{Dis}}}{Cap_{ds}^{B}}\Delta t \tag{d4}$$

$$SOC_{ds,t=0}^{B}=SOC_{ds,t=24}^{B}=SOC^{B,Initial} \tag{d5}$$

$$SOC^{\min}\leq SOC_{ds,t}^{B}\leq SOC^{\max} \tag{d6}$$

- **Linear AC Power Flow**

To manage power flow in DSs, a linear AC power flow program is embedded into the model [39]. The equations needed to calculate the flow of active and reactive powers in each branch are respectively

presented in Eqs. (e1) and (e2). G_l and B_l , respectively, refer to the conductance and susceptance of branch l. The magnitude and angle of voltage at node i are respectively indicated by $V_{i,t}$ and $\theta_{i,t}$. The power loss of branch l is calculated based on the flow of its active and reactive powers, as shown in Eq. (e3). Equation (e4) confines the flow of active and reactive powers in each branch of DSs to the maximum apparent power flow ($S_l^{Line,\max}$). Equations (e5) and (e6) are respectively provided to prevent the magnitude and voltage angle from exceeding the safe range. To avoid the imbalance of active and reactive powers in each node, respectively, Eqs. (e7) and (e8) are provided. These equations guarantee the equality of power injection and extraction in each node. Lastly, Eq. (e9) applies the power flow constraint in the tie-line between the DS and TS. Note that Eqs. (e4) and (e9) are linearized by dodecagon approximation method [40].

$$P_{l,t}^{Line} = G_l\left(V_{i,t} - V_{j,t}\right) + B_l\left(\theta_{i,t} - \theta_{j,t}\right) \tag{e1}$$

$$Q_{l,t}^{Line} = B_l\left(V_{i,t} - V_{j,t}\right) - G_l\left(\theta_{i,t} - \theta_{j,t}\right) \tag{e2}$$

$$P_{l,t}^{Loss} = R_l\left[\left(P_{l,t}^{Line}\right)^2 + \left(Q_{l,t}^{Line}\right)^2\right] \tag{e3}$$

$$0 \le \left(P_{l,t}^{Line}\right)^2 + \left(Q_{l,t}^{Line}\right)^2 \le \left(S_l^{Line,\max}\right)^2 \tag{e4}$$

$$V^{\min} \le V_{i,t} \le V^{\max} \tag{e5}$$

$$\theta^{\min} \le \theta_{i,t} \le \theta^{\max} \tag{e6}$$

$$\begin{aligned}&\left(P_{d,t}^{PCC} + P_{d,t}^{PCC,up} - P_{d,t}^{PCC,down}\right)\Big|_{i=d} + \sum_{dg\in\Delta_i^g}\left(P_{dg,t}^{DG} + \Delta P_{dg,t,sc}^{GT,up} - \Delta P_{dg,t,sc}^{GT,down}\right)\\ &+ \sum_{ds\in\Delta_i^{ds}}\left(P_{ds,t}^{B,Dis} - P_{ds,t}^{B,Ch} + \Delta P_{ds,t}^{B,up} - \Delta P_{ds,t}^{B,down}\right) = \sum_{l\in\Delta_d^l}\left(\xi_{l,i}P_{l,t}^{Line} + \frac{P_{l,t}^{Loss}}{2}\right) + \sum_{b\in\Delta_i^b} P_{b,t}^{Net} + P_{i,t}^{Load}\end{aligned} \tag{e7}$$

$$Q_{d,t}^{PCC}\Big|_{i=d} + \sum_{dg\in\Delta_{(d,i)}^{dg}} Q_{dg,t}^{GT} = \sum_{l\in\Delta_d^l}\xi_{l,i}Q_{l,t}^{Line} + \sum_{b\in\Omega_{(d,i)}^b}\tan\left(\varphi_i\right)P_{b,t}^{Net} + Q_{i,t}^{Load} \tag{e8}$$

$$0 \le \left(P_{d,t}^{PCC}\right)^2 + \left(Q_{d,t}^{PCC}\right)^2 \le \left(S_d^{Line,\max}\right)^2 \tag{e9}$$

2.2. Lower-Level (TSO Optimization)

In this sub-section, the lower-level of the proposed framework is formulated where the transmission system operational planning is done by the TSO. The objective function of the TSO is given in Eq. (5) while its operating constraints are formulated in (f1)-(h3). Note that a dual variable is assigned to each of

the TSO operation constraints as it is needed for the dual modeling of the TSO operation problem. As per (5), the objective function of TSO is to minimize the DA operation costs of the TS. The first and second terms of this function respectively calculate the power purchase costs from thermal units (Tus) and BESSs placed in TS with regard to their participation in the energy and flexibility markets.

$$OF^{TSO} = \min \sum_{t} \left\{ \begin{array}{l} \sum_{g} \left[\pi_{g}^{TU} P_{g,t}^{TU} + \pi_{g}^{TU,flex} \left(\Delta P_{g,t}^{TU,up} + \Delta P_{g,t}^{TU,down} \right) \right] \\ + \sum_{s} \left[\pi_{s}^{B} \left(P_{s,t}^{B,Ch} + P_{s,t}^{B,Dis} \right) + \pi_{s}^{B,flex} \left(\Delta P_{s,t}^{B,up} + \Delta P_{s,t}^{B,down} \right) \right] \end{array} \right\} \quad (5)$$

- **Generation Units**

Eqs. (f1) to (f4) formulate the operation of transmission-wide generation units. Wind farms and centralized PV farms placed in the transmission system are modeled in Eqs. (f1) and (f2). These equations are similar to Eqs. (c1) and (c2) and only their indices have been updated. Condition (f3) confines the upper and lower levels of the operating point of TUs according to their participation in the energy ($P_{g,t}^{TU}$) and flexibility ($\Delta P_{g,t}^{TU,up}$ / $\Delta P_{g,t}^{TU,down}$) markets. Finally, Condition (f4) expresses that the operating point of TUs is bounded by ramp-up and ramp-down limits.

$$P_{g,t}^{W} = \begin{cases} 0 & , \ v_t < v_{ci} \quad \text{Or} \ \ v_t \geq v_{co} \\ P_{g}^{W,\max} \left(\dfrac{v_t^2 - v_{ci}^2}{v_r^2 - v_{ci}^2} \right) & , \ v_{ci} \leq v_t < v_r \\ P_{g}^{W,\max} & , \ v_r \leq v_t < v_{co} \end{cases} \quad (f1)$$

$$P_{g,t}^{PV} = \eta^{PV} \frac{G_t}{G^{STD}} P_{g}^{PV,\max} \quad (f2)$$

$$P_{g}^{TU,\min} \leq P_{g,t}^{TU} + \Delta P_{g,t}^{TU,up} - \Delta P_{g,t}^{TU,down} \leq P_{g}^{TU,\max} \ , \ \left(\psi_{g,t}^{\min}, \psi_{g,t}^{\max} \right) \quad (f3)$$

$$-P_{g}^{RD} + \Delta P_{g,t}^{TU,down} \leq P_{g,t}^{TU} - P_{g,t-1}^{TU} \leq P_{g}^{RU} - \Delta P_{g,t}^{TU,up} \ , \ \left(\upsilon_{g,t}^{\min}, \upsilon_{g,t}^{\max} \right) \quad (f4)$$

- **Transmission-Wide Battery Energy Storage Systems**

Constraints (g1)-(g5) are presented to model transmission-wide BESSs. In this way, constraints (g1) and (g2) respectively confine the participation of BESS in energy and flexibility markets. The SoC of BESS at hour 1 is calculated by Eq. (g3) while at hours 2 to 23 it is calculated by Eq. (g4). Note that SoC is set

to a fixed value at 0 and 24 hours. Condition (g5) prevents BESS energy level from exceeding the allowed range.

$$0 \le P_{s,t}^{B,Dis} + \Delta P_{s,t}^{B,up} \le P_s^{Dis,\max} \ , \ \left(\xi_{s,t}^{\min}, \xi_{s,t}^{\max}\right) \tag{g1}$$

$$0 \le P_{s,t}^{B,Ch} + \Delta P_{s,t}^{B,down} \le P_s^{Ch,\max} \ , \ \left(\zeta_{s,t}^{\min}, \zeta_{s,t}^{\max}\right) \tag{g2}$$

$$E_{s,t}^{B} = E_s^{B,Initial} + \left(\eta^{Ch}\left(P_{s,t}^{B,Ch} + \Delta P_{s,t}^{B,down}\right) - \frac{\left(P_{s,t}^{B,Dis} + \Delta P_{s,t}^{B,up}\right)}{\eta^{Dis}} \right) \Delta t \ , \ \varsigma_{s,t}^{B} \qquad \forall s, \forall t = 1 \tag{g3}$$

$$E_{s,t}^{B} = E_{s,t-1}^{B} + \left(\eta^{Ch}\left(P_{s,t}^{B,Ch} + \Delta P_{s,t}^{B,down}\right) - \frac{\left(P_{s,t}^{B,Dis} + \Delta P_{s,t}^{B,up}\right)}{\eta^{Dis}} \right) \Delta t \ , \ \varsigma_{s,t}^{B} \qquad \forall s, \forall t \in [2,24) \tag{g4}$$

$$E_s^{\min} \le E_{ds,t}^{B} \le E_s^{\max} \ , \ \left(\tau_{s,t}^{\min}, \tau_{s,t}^{\max}\right) \tag{g5}$$

- **DC Power Flow**

The DC power flow program executed at TS is formulated through (h1)-(h3). Equations (h1) and (h2) guarantee energy and flexibility balances in each bus of the TS, respectively. The power passing through the line l is confined by the condition (h3) based on the generation shift factors (GSFs) [13]. It is noteworthy to state that production and consumption are respectively modeled with positive and negative signs in (h3).

$$\sum_g P_{g,t}^{TU} + \sum_s \left(P_{s,t}^{B,Dis} - P_{s,t}^{B,Ch}\right) = \sum_n P_{n,t}^{Demand} + \sum_d P_{d,t}^{PCC} \ , \ \omega_t^{LMP} \tag{h1}$$

$$\sum_g \left(\Delta P_{g,t}^{TU,up} - \Delta P_{g,t}^{TU,down}\right) + \sum_s \left(\Delta P_{s,t}^{B,up} - \Delta P_{s,t}^{B,down}\right) = \sum_n \Delta P_{n,t}^{Demand} + \sum_d \left(P_{d,t}^{PCC,up} - P_{d,t}^{PCC,down}\right) \ , \ \omega_t^{FLMP} \tag{h2}$$

$$\begin{aligned} -S_l^{Line,\max} \le & \sum_g \left[GSF_{l,g}\left(P_{g,t}^{TU} + \Delta P_{g,t}^{TU,up} - \Delta P_{g,t}^{TU,down}\right)\right] \\ & + \sum_s \left[GSF_{l,s}\left(P_{s,t}^{B,Dis} - P_{s,t}^{B,Ch} + \Delta P_{s,t}^{B,up} - \Delta P_{s,t}^{B,down}\right)\right] \\ & - \sum_n \left[GSF_{l,n}\left(P_{n,t}^{Demand} + \Delta P_{n,t}^{Demand}\right)\right] \\ & - \sum_d \left[GSF_{l,d}\left(P_{d,t}^{PCC} + P_{d,t}^{PCC,up} - P_{d,t}^{PCC,down}\right)\right] \le S_l^{Line,\max} \ , \ \left(\mu_{l,t}^{\min}, \mu_{l,t}^{\max}\right) \end{aligned} \tag{h3}$$

- **Calculation of Locational Marginal Price**

Equations (i1) and (i2) calculate respectively LMP and FLMP of different buses of the transmission network according to binary variables related to equations (h1)-(h3) [41]. These equations show that the

LMP / FLMP of each bus consists of two parts. The first part of these equations is related to the hourly price of energy / flexibility regardless of location while their second parts calculate the change in energy / flexibility price in different buses according to power flow constraints.

$$\pi_{n,t}^{LMP} = \omega_t^{LMP} + \sum_l \left[GSF_{l,n} \left(\mu_{l,t}^{\min} - \mu_{l,t}^{\max} \right) \right] \quad \text{(i1)}$$

$$\pi_{n,t}^{FLMP} = \omega_t^{FLMP} + \sum_l \left[GSF_{l,n} \left(\mu_{l,t}^{\min} - \mu_{l,t}^{\max} \right) \right] \quad \text{(i2)}$$

2-5- Converting the bi-level NLP problem to single-level LP problem

As mentioned above, the introduced bi-level model is a non-convex problem since the DSO objective function has a non-linear term (Eq. 4). Therefore, the bi-level model should be converted into a convergent problem that can be tracked by linear solvers such as CPLEX, GUROBI, and so on. To this end, we first convert the bi-level model into a single-level mathematical program with equilibrium constraints (MPEC) by replacing its lower-level (TSO operational planning problem) with KKT conditions. Then we use the Big-M technique to linearize KKT conditions, and SDT to linearize the nonlinear term of the DSO objective function. Therefore, the final model will be a single-level MPEC problem including primal-dual constraints.

2.5.1. Dual Constraints of the TSO's Optimization Problem

The dual formulation of the lower-level problem is presented below. In this way, Eqs. (j1)-(j8) present the first-order partial derivative of the Lagrange function of the lower-level problem. It should be stated that the constant value of the right-hand side (RHS) of the dual constraints are the coefficients of TSO objective function variables.

$$\psi_{g,t}^{\min} - \psi_{g,t}^{\max} + \upsilon_{g,t}^{\min} - \upsilon_{g,t+1}^{\min} - \upsilon_{g,t}^{\max} + \upsilon_{g,t+1}^{\max} + \omega_t^{LMP} + \sum_l \left[GSF_{l,g} \left(\mu_{l,t}^{\min} - \mu_{l,t}^{\max} \right) \right] = \pi_g^G \quad \text{(j1)}$$

$$\psi_{g,t}^{\min} - \psi_{g,t}^{\max} - \upsilon_{g,t}^{\max} + \omega_t^{FLMP} + \sum_l \left[GSF_{l,g} \left(\mu_{l,t}^{\min} - \mu_{l,t}^{\max} \right) \right] = \pi_g^{TU,flex} \quad \text{(j2)}$$

$$\psi_{g,t}^{\max} - \psi_{g,t}^{\min} - \upsilon_{g,t}^{\min} - \omega_t^{FLMP} + \sum_l \left[GSF_{l,g} \left(\mu_{l,t}^{\max} - \mu_{l,t}^{\min} \right) \right] = \pi_g^{TU,flex} \quad \text{(j3)}$$

$$\xi_{s,t}^{\min} - \xi_{s,t}^{\max} + \frac{\varsigma_{s,t}^B}{\eta^{Dis}} \Delta t + \omega_t^{LMP} + \sum_l \left[GSF_{l,s} \left(\mu_{l,t}^{\min} - \mu_{l,t}^{\max} \right) \right] = \pi_s^B \quad \text{(j4)}$$

$$\zeta_{s,t}^{\min} - \zeta_{s,t}^{\max} - \varsigma_{s,t}^{B}\eta^{Ch}\Delta t - \omega_t^{LMP} + \sum_l \left[GSF_{l,g}\left(\mu_{l,t}^{\max} - \mu_{l,t}^{\min}\right)\right] = \pi_s^{B} \quad \text{(j5)}$$

$$\xi_{s,t}^{\min} - \xi_{s,t}^{\max} + \frac{\varsigma_{s,t}^{B}}{\eta^{Dis}}\Delta t + \omega_t^{FLMP} + \sum_l \left[GSF_{l,s}\left(\mu_{l,t}^{\min} - \mu_{l,t}^{\max}\right)\right] = \pi_s^{B,\,flex} \quad \text{(j6)}$$

$$\zeta_{s,t}^{\min} - \zeta_{s,t}^{\max} - \varsigma_{s,t}^{B}\eta^{Ch}\Delta t - \omega_t^{FLMP} + \sum_l \left[GSF_{l,g}\left(\mu_{l,t}^{\max} - \mu_{l,t}^{\min}\right)\right] = \pi_s^{B,\,flex} \quad \text{(j7)}$$

$$\varsigma_{s,t}^{B} - \varsigma_{s,t+1}^{B} + \tau_{s,t}^{\min} - \tau_{s,t}^{\max} = 0 \quad \text{(j8)}$$

2.5.2. KKT Conditions

In (k1)-(k12) complementary relaxation constraints are modeled for inequality constraints to embed KKT conditions in the model [42]. In the proposed formulation, we assume that all the binary variables of inequality constraints are positive. Note that the perpendicular symbol ($\perp$) refers to the complementary condition.

$$0 \le \psi_{g,t}^{\min} \perp P_{g,t}^{TU} + \Delta P_{g,t}^{TU,up} - \Delta P_{g,t}^{TU,down} - P_g^{TU,\min} \ge 0 \quad \text{(k1)}$$

$$0 \le \psi_{g,t}^{\max} \perp P_g^{TU,\max} - P_{g,t}^{TU} - \Delta P_{g,t}^{TU,up} + \Delta P_{g,t}^{TU,down} \ge 0 \quad \text{(k2)}$$

$$0 \le \upsilon_{g,t}^{\min} \perp P_{g,t}^{TU} - P_{g,t-1}^{TU} + P_g^{RD} - \Delta P_{g,t}^{TU,down} \ge 0 \quad \text{(k3)}$$

$$0 \le \upsilon_{g,t}^{\max} \perp P_g^{RU} - \Delta P_{g,t}^{TU,up} - P_{g,t}^{TU} + P_{g,t-1}^{TU} \ge 0 \quad \text{(k4)}$$

$$0 \le \xi_{s,t}^{\min} \perp P_{s,t}^{B,Dis} + \Delta P_{s,t}^{B,up} \ge 0 \quad \text{(k5)}$$

$$0 \le \xi_{s,t}^{\max} \perp P_s^{Dis,\max} - P_{s,t}^{B,Dis} - \Delta P_{s,t}^{B,up} \ge 0 \quad \text{(k6)}$$

$$0 \le \zeta_{s,t}^{\min} \perp P_{s,t}^{B,Ch} + \Delta P_{s,t}^{B,down} \ge 0 \quad \text{(k7)}$$

$$0 \le \zeta_{s,t}^{\max} \perp P_s^{Ch,\max} - P_{s,t}^{B,Ch} - \Delta P_{s,t}^{B,down} \ge 0 \quad \text{(k8)}$$

$$0 \le \tau_{s,t}^{\min} \perp E_{ds,t}^{B} - E_s^{\min} \ge 0 \quad \text{(k9)}$$

$$0 \le \tau_{s,t}^{\max} \perp E_s^{\max} - E_{ds,t}^{B} \ge 0 \quad \text{(k10)}$$

$$\begin{aligned} 0 \le \mu_{l,t}^{\min} \perp & \sum_g \left[GSF_{l,g}\left(P_{g,t}^{TU} + \Delta P_{g,t}^{TU,up} - \Delta P_{g,t}^{TU,down}\right)\right] \\ & + \sum_s \left[GSF_{l,s}\left(P_{s,t}^{B,Dis} - P_{s,t}^{B,Ch} + \Delta P_{s,t}^{B,up} - \Delta P_{s,t}^{B,down}\right)\right] \\ & - \sum_n \left(GSF_{l,n}P_{n,t}^{Demand}\right) - \sum_d \left[GSF_{l,d}\left(P_{d,t}^{PCC} + P_{d,t}^{PCC,up} - P_{d,t}^{PCC,down}\right)\right] + S_l^{Line,\max} \ge 0 \end{aligned} \quad \text{(k11)}$$

$$\begin{aligned} 0 \le \mu_{l,t}^{\max} \perp & S_l^{Line,\max} - \sum_g \left[GSF_{l,g}\left(P_{g,t}^{TU} + \Delta P_{g,t}^{TU,up} - \Delta P_{g,t}^{TU,down}\right)\right] \\ & - \sum_s \left[GSF_{l,s}\left(P_{s,t}^{B,Dis} - P_{s,t}^{B,Ch} + \Delta P_{s,t}^{B,up} - \Delta P_{s,t}^{B,down}\right)\right] \\ & + \sum_n \left(GSF_{l,n}P_{n,t}^{Demand}\right) + \sum_d \left[GSF_{l,d}\left(P_{d,t}^{PCC} + P_{d,t}^{PCC,up} - P_{d,t}^{PCC,down}\right)\right] \ge 0 \end{aligned} \quad \text{(k12)}$$

2.5.3. Linearization of the KKT Conditions

Eqs. (l1)-(l3) make the above nonlinear complementary conditions linear by Big-M method [42]. In this method, an auxiliary binary variable (g) is defined. The value of the binary variable g is determined according to the fulfilled complementary condition. In order to use the Big-M method for linearization, it is necessary to write all inequality constraints with a positive sign, as done in constraints (k1)-(k12).

$$0 \le a \perp b \ge 0 \quad \text{(l1)}$$
$$0 \le a \le gM \quad \text{(l2)}$$
$$0 \le b \le (1-g)M \quad \text{(l3)}$$

2.5.4. Strong Duality Theory

In this subsection, SDT is used to linearize the non-linear term of the DSO objective function (referring to Eq. 4) where energy / flexibility price and power / flexibility exchange rate at coupling nodes are variable. According to SDT, the value of the lower-level objective function (TSO objective function) must be equal to the dual objective function [43]. Eq. (m1) is provided to model this rule. Then, Eq. (m2) is built by embedding Eqs. (i1) and (i2) in Eq. (m1). As can be seen, the non-linear term of the upper-level objective function (DSO objective function) is extracted and written at the left-hand side (LHS) of the Eq. (m2), while its equivalent linear relationship is presented at the RHS. Therefore, the nonlinear term can be replaced with its equivalent linear relation in the upper-level objective function. In this way, the objective function of the single-level MPEC model (m3) is built by replacing the non-linear term of the upper-level objective function (Eq. 4) with the linear term obtained in (m2). Lastly, all constraints required to solve the objective function (m3) including KKT conditions, and primal and dual constraints are shown in (m4).

$$
\begin{aligned}
&\sum_t \left\{ \begin{array}{l} \sum_g \left[\pi_g^{TU} P_{g,t}^{TU} + \pi_g^{TU,\,flex} \left(\Delta P_{g,t}^{TU,up} + \Delta P_{g,t}^{TU,down} \right) \right] \\ + \sum_s \left[\pi_s^{B} \left(P_{s,t}^{B,Ch} + P_{s,t}^{B,Dis} \right) + \pi_s^{B,\,flex} \left(\Delta P_{s,t}^{B,up} + \Delta P_{s,t}^{B,down} \right) \right] \end{array} \right\} = \\
&+ \sum_t \sum_g \left(P_g^{TU,\min} \psi_{g,t}^{\min} - P_g^{TU,\max} \psi_{g,t}^{\max} - P_g^{RD} \upsilon_{g,t}^{\min} - P_g^{RU} \upsilon_{g,t}^{\max} \right) \\
&+ \sum_t \sum_s \left(E_s^{B,Initial} \varsigma_{s,t}^{B} + E_s^{\min} \tau_{s,t}^{\min} - E_s^{\max} \tau_{s,t}^{\max} - P_s^{Dis,\max} \xi_{s,t}^{\max} - P_s^{Ch,\max} \zeta_{s,t}^{\max} \right) \\
&+ \sum_t \sum_l \left\langle \left\{ \begin{array}{l} \sum_n \left[GSF_{l,n} \left(P_{n,t}^{Demand} + \Delta P_{n,t}^{Demand} \right) \right] \\ + \sum_d \left[GSF_{l,d} \left(P_{d,t}^{PCC} + P_{d,t}^{PCC,up} - P_{d,t}^{PCC,down} \right) \right] - S_l^{Line,\max} \end{array} \right\} \mu_{l,t}^{\min} \right\rangle \\
&- \sum_t \sum_l \left\langle \left\{ \begin{array}{l} \sum_n \left[GSF_{l,n} \left(P_{n,t}^{Demand} + \Delta P_{n,t}^{Demand} \right) \right] \\ + \sum_d \left[GSF_{l,d} \left(P_{d,t}^{PCC} + P_{d,t}^{PCC,up} - P_{d,t}^{PCC,down} \right) \right] + S_l^{Line,\max} \end{array} \right\} \mu_{l,t}^{\max} \right\rangle \\
&+ \sum_t \left[\left(\sum_n P_{n,t}^{Demand} + \sum_d P_{d,t}^{PCC} \right) \omega_t^{LMP} \right] \\
&+ \sum_t \left[\left(\sum_n \Delta P_{n,t}^{Demand} + \sum_d \left(P_{d,t}^{PCC,up} - P_{d,t}^{PCC,down} \right) \right) \omega_t^{FLMP} \right]
\end{aligned}
\tag{m1}
$$

$$
\begin{aligned}
&\sum_t \sum_d \left[P_{d,t}^{PCC} \pi_{d,t}^{LMP} - \left(P_{d,t}^{PCC,up} \pi_{d,t}^{FLMP,up} + P_{d,t}^{PCC,down} \pi_{d,t}^{FLMP,down} \right) \right] = \\
&\sum_t \left\{ \begin{array}{l} \sum_g \left[\pi_g^{TU} P_{g,t}^{TU} + \pi_g^{TU,\,flex} \left(\Delta P_{g,t}^{TU,up} + \Delta P_{g,t}^{TU,down} \right) \right] \\ + \sum_s \left[\pi_s^{B} \left(P_{s,t}^{B,Ch} + P_{s,t}^{B,Dis} \right) + \pi_s^{B,\,flex} \left(\Delta P_{s,t}^{B,up} + \Delta P_{s,t}^{B,down} \right) \right] \end{array} \right\} \\
&- \sum_t \sum_g \left(P_g^{TU,\min} \psi_{g,t}^{\min} - P_g^{TU,\max} \psi_{g,t}^{\max} - P_g^{RD} \upsilon_{g,t}^{\min} - P_g^{RU} \upsilon_{g,t}^{\max} \right) \\
&- \sum_t \sum_s \left(E_s^{B,Initial} \varsigma_{s,t}^{B} + E_s^{\min} \tau_{s,t}^{\min} - E_s^{\max} \tau_{s,t}^{\max} - P_s^{Dis,\max} \xi_{s,t}^{\max} - P_s^{Ch,\max} \zeta_{s,t}^{\max} \right) \\
&- \sum_t \sum_l \left\langle \left\{ \begin{array}{l} \sum_n \left[GSF_{l,n} \left(P_{n,t}^{Demand} + \Delta P_{n,t}^{Demand} \right) \right] \\ - S_l^{Line,\max} \end{array} \right\} \mu_{l,t}^{\min} \right\rangle \\
&+ \sum_t \sum_l \left\langle \left\{ \begin{array}{l} \sum_n \left[GSF_{l,n} \left(P_{n,t}^{Demand} + \Delta P_{n,t}^{Demand} \right) \right] \\ + S_l^{Line,\max} \end{array} \right\} \mu_{l,t}^{\max} \right\rangle \\
&- \sum_t \left[\sum_n P_{n,t}^{Demand} \omega_t^{LMP} \right] - \sum_t \left[\sum_n \Delta P_{n,t}^{Demand} \omega_t^{FLMP} \right]
\end{aligned}
\tag{m2}
$$

$$
\begin{aligned}
OF^{MPEC} = \min \sum_{d}\sum_{t}\Bigg[& \sum_{dg\in\Delta_d^{dg}}\left(\pi_{dg}^{GT}P_{dg,t}^{DG}+\pi_{dg}^{GT,flex}\Delta P_{dg,t}^{GT,up}+\pi_{dg}^{GT,flex}\Delta P_{dg,t}^{GT,down}\right) \\
& +\sum_{ds\in\Delta_d^{ds}}\left[\pi_{ds}^{B}P\left(P_{ds,t}^{B,Ch}+P_{ds,t}^{B,Dis}\right)+\pi_{ds}^{B,flex}\Delta P_{ds,t}^{B,up}+\pi_{ds}^{B,flex}\Delta P_{ds,t}^{B,down}\right]\Bigg] \\
& \sum_{t}\left\{\begin{array}{l}\sum_{g}\left[\pi_{g}^{TU}P_{g,t}^{TU}+\pi_{g}^{TU,flex}\left(\Delta P_{g,t}^{TU,up}+\Delta P_{g,t}^{TU,down}\right)\right] \\ +\sum_{s}\left[\pi_{s}^{B}\left(P_{s,t}^{B,Ch}+P_{s,t}^{B,Dis}\right)+\pi_{s}^{B,flex}\left(\Delta P_{s,t}^{B,up}+\Delta P_{s,t}^{B,down}\right)\right]\end{array}\right\} \\
& -\sum_{t}\sum_{g}\left(P_{g}^{TU,\min}\psi_{g,t}^{\min}-P_{g}^{TU,\max}\psi_{g,t}^{\max}-P_{g}^{RD}\upsilon_{g,t}^{\min}-P_{g}^{RU}\upsilon_{g,t}^{\max}\right) \\
& -\sum_{t}\sum_{s}\left(E_{s}^{B,Initial}\varsigma_{s,t}^{B}+E_{s}^{\min}\tau_{s,t}^{\min}-E_{s}^{\max}\tau_{s,t}^{\max}-P_{s}^{Dis,\max}\xi_{s,t}^{\max}-P_{s}^{Ch,\max}\zeta_{s,t}^{\max}\right) \\
& -\sum_{t}\sum_{l}\left\langle\left\{\begin{array}{l}\sum_{n}\left[GSF_{l,n}\left(P_{n,t}^{Demand}+\Delta P_{n,t}^{Demand}\right)\right] \\ -S_{l}^{Line,\max}\end{array}\right\}\mu_{l,t}^{\min}\right\rangle \\
& +\sum_{t}\sum_{l}\left\langle\left\{\begin{array}{l}\sum_{n}\left[GSF_{l,n}\left(P_{n,t}^{Demand}+\Delta P_{n,t}^{Demand}\right)\right] \\ +S_{l}^{Line,\max}\end{array}\right\}\mu_{l,t}^{\max}\right\rangle \\
& -\sum_{t}\left[\sum_{n}P_{n,t}^{Demand}\omega_{t}^{LMP}\right]-\sum_{t}\left[\sum_{n}\Delta P_{n,t}^{Demand}\omega_{t}^{FLMP}\right]
\end{aligned}
\tag{m3}
$$

$$
\begin{aligned}
& s.t. \\
& \text{(c1-c4),(d1-d6),(e1-e9),(f1-f4),(g1-g5),(h1-h3),(j1-j8),(k1-k12)}
\end{aligned}
\tag{m4}
$$

2.6. Two-Stage Interval-Based Optimization Algorithm

To secure the proposed nested framework against the uncertainties associated with RGs output power and load consumption, a two-stage interval-based optimization algorithm is used. The advantages of the interval-based technique include a smaller computing space compared to the stochastic technique and achieving more optimal results than the robust technique due to minimizing the interval of the objective function instead of considering the worst-case scenario [44]. In stage 1 of the proposed interval-based model, the single-level MPEC problem constructed in the Section 2-5 is solved in an iteration-based process to determine the final values of the variables of the single-level MPEC problem, except the variables related to BESSs. Then, in Stage 2, the final operating points of BESSs are determined by considering extreme conditions, so operational planning will also be applicable for the worst conditions.

Equations (n1)-(n3) are needed to model the aforementioned process. Equation (n1) divides the variables and parameters of the problem into three categories. x refers to all variables of the single-level MPEC problem except BESSs variables; y refers to BESSs variables; u refers to uncertain parameters including load demand, solar radiation and wind speed. In Eq. (n2), an uncertainty interval is determined for each of the uncertain parameters. Note that the upper and lower limits of this range are set to 0.8 and 1.2 of expected values for wind speed and solar radiation, while they are set to 0.9 and 1.1 of expected values for load demand. Eventually, Eq. (n3) shows the general form of solving single-level MPEC problem by the proposed interval-based optimization technique.

$$x \in \{\text{Variable of single-level MPEC problem except distribution- and transmission-wide BESSs}\}$$
$$y \in \{\text{Variables of distribution- and transmission-wide BESSs}\} \quad \text{(n1)}$$
$$u \in \{\text{Wind speed, Sun irradiance, Load}\}$$

$$u^{\min} \le u \le u^{\max} \quad \text{(n2)}$$

$$\min_{x,y}\left[\max_{u} \text{ or } \min_{u} F(x,y,u)\right]$$
$$s.t. \quad \text{(n3)}$$
$$G(x,y,u) = 0$$
$$H(x,y,u) \le 0$$

3. Solution Method

Figure 2 depicts the implementation process of the proposed nested framework. First, it should be mentioned that the proposed nested framework is coded in the GAMS environment where the CPLEX solver is used to solve it. According to Fig. 2, after submitting the input parameters to the GAMS, the first layer of the upper-level, which is the design of time-varying DRP tariffs, is modeled. Then the designed tariffs are sent to EMS of SBs to do their DA scheduling in the second layer of the upper-level. After scheduling SBs, their DA hourly load demand is determined and sent to the DSO to plan the operation of the DS in the third layer of the upper-level. After the DA planning of the DS, the upper-level is completed and the DSO sends its obtained schedule to the lower-level. In the lower-level, TSO performs the DA operational planning of the TS. Since the objective function of DSO is non-linear, the third layer of the upper-level and lower-level are merged to form a single-level MPEC problem.

According to the flowchart, the process of converting the NLP bi-level problem to the single-level MPEC problem is done in four steps; In step 1, the dual form of the lower-level problem is written. In step 2, complementary relaxation constraints are modeled to embed KKT conditions in the formulation. In step 3, the nonlinear complementary conditions are linearized via the Big-M method. Finally, in step 4, the non-linear term of the DSO objective function is linearized using SDT.

According to the right side of the flowchart, in order to secure the operational planning of TSO-DSO against uncertainties, the obtained single-level MPEC problem is solved by using an interval-based two-stage optimization algorithm. According to the flowchart, in the first iteration, all variables of the single-level MPEC problem are calculated by setting the uncertain parameters on the deterministic values. Then, the single-level MPEC problem is solved by fixing all the variables on their values obtained in the previous step, and considering the uncertain parameters as variables in both pessimistic and optimistic fashions. In the next step, the stop criterion is checked, if it is satisfied, the solution process is stopped, otherwise, the uncertain parameters are set to the values obtained from pessimistic programming, and then the solution process enters the next iteration. It should be noted that after satisfying the stop criterion, all variables of the problem are fixed on their results obtained in the last iteration except the BESSs' variables, and the single-level problem is solved in stage 2 for extreme conditions. In this stage, the values of BESSs variables are determined according to extreme conditions. To facilitate the simulation of the proposed nested framework, a pseudocode is presented in Table 1, in which each part of the proposed framework is described separately.

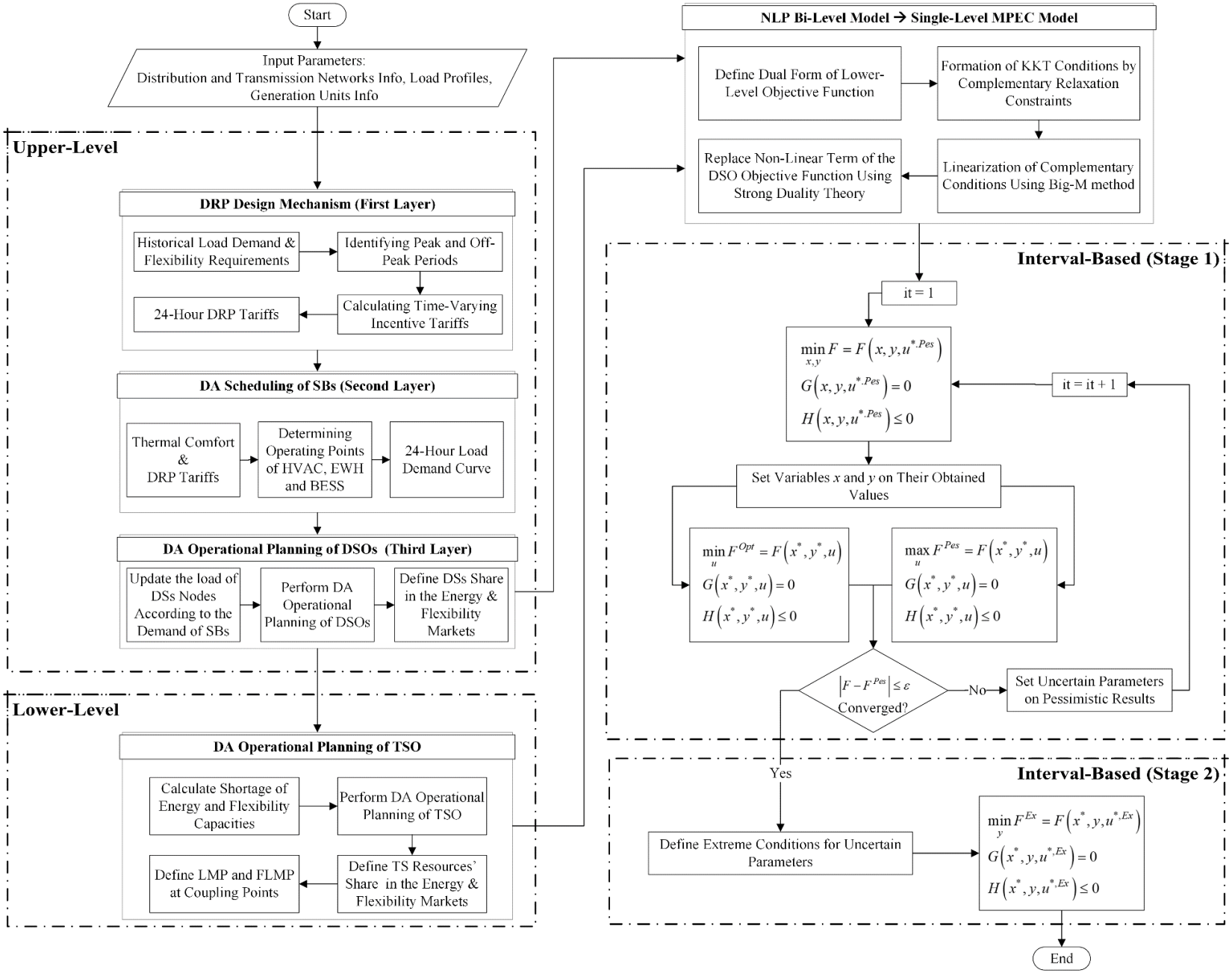

Fig. 2. Flowchart of the proposed interval-based nested framework

Table 1. Pseudocode to implement the proposed nested framework

Upper-Level	**DR Design (Layer 1)**	**For** each SB ***b***, **Do**: **For** each hour ***t***, **Do**: **If** flexibility requirement is Positive, **Then**: Define maximum load decrement rate [Eq. (1)]. Define incentive tariff based on upward flexibility requirement [Eq. (1)]. **Else**, Define maximum load increment rate [Eq. (2)]. Define time-varying tariffs based on downward flexibility requirement [Eq. (2)]. **End** **End** **Return** Designed DRP with time-varying tariffs for SB ***b***. **End**
	SBs Scheduling (Layer 2)	**For** each SB ***b***, **Do**: Set Maximum load increment and decrement rates for SB ***b*** [Eqs. (a5)-(a6)]. Set thermal comforts based on desired temperatures for indoor space and hot water [Eqs. (a10),(a17),(a19)-(a20)]. Solve the objective function of SBs [Eq. (3)]. **Return** Schedule obtained for SB ***b***. **End**
	DSs Operation (Layer 3)	**For** each SB ***b***, **Do**: Update demand curve of SB ***b*** based-on its obtained schedule. **End** Define Linear AC power flow to manage power transfer in DSs [Eqs. (e1)-(e9)]. Solve the DSOs objective function [Eq. (4)]. **Return** Energy/Flexibility market participation of DSOs.
Lower-Level	**TS Operation**	**For** each DS ***d***, **Do**: Set energy shortage/surplus and flexibility coverage level. Define DC power flow to manage power transfer in TS [Eqs. (h1)-(h3)]. **End** Solve the TSO objective function [Eq. (5)].
Single-Level MPEC Formation	**Dual Constraints of Lower-Level**	Set dual variables for active constraints in TSO optimization problem [Eqs. (j1)-(j8)]. Define dual constraints based-on variables in TSO optimization problem and their coefficients in the objective function.
	KKT Conditions	**For** each dual variable and its corresponding primal constraints, **Do**: Define a complementary condition [Eqs. (k1)-(k12)]. **End**
	Big-M Linearization	**For** each complementary condition, **Do**: Define an auxiliary binary variable ***g***. Replace each complementary condition with its linearized equivalent using Big-M Method [Eqs. (l1)-(l3)]. **End**
	Strong Duality Theory	Define dual objective function of lower-level problem [Eqs. (m1)-(m2)]. Solve the strong duality condition to extract non-linear term of the upper-level objective function [Eqs. (m3)-(m4)].
Two-Stage Interval-Based Optimization Algorithm	**Stage 1**	**For** each uncertain parameter ***u***, **Do**: Define upper and lower limits. **End** **While** 1, **Do**: **If** it's the first iteration, **Then**: Set the counter number ***it*** to 1. Set uncertain parameters ***u*** in their deterministic values. **Else**, Increase the counter number ***it*** by one unit. Set uncertain parameters ***u*** in their pessimistic obtained results. **End** Free up decision variables ***x*** and ***y***. Solve single-level MPEC model. Set variables ***x*** and ***y*** on their obtained values. Free up uncertain parameters ***u***. Solve optimistic form of the single-level MPEC model. Solve pessimistic form of single-level MPEC model. **If** stopping criteria reached, **Then**: **Break**. **End** **End** **Return** final result of variables ***x***.
	Stage 2	Define extreme condition by setting following adjustments: $\boldsymbol{u}^{gen}$ → Set to minimum values. $\boldsymbol{u}^{demand}$ → Set to maximum values. Set variables ***x*** at their results obtained from stage 1. Solve extreme form of the single-level MPEC model. **Return** operating points of BESSs.

4. Simulation of the Proposed Framework

4.1. Studied System

Figure 3 shows the structure of the studied system on which the proposed nested framework is implemented. This system consists of a 57-bus TS coupled with two 33-node [41] DSs. In this system, energy and flexibility markets are cleared in a coordinated structure based on interactions between TSO and DSOs. The TS has traditional TUs, wind farms and Solar farms, while DSs are equipped with GTs, wind turbines and centralized PV plants. It should be mentioned that RGs at both transmission and distribution levels are integrated with BESSs. There are two categories of DS' loads; A) Regular loads (RLs) B) SBs. The components of SBs are also shown in Fig. 3. Thermostatically-controlled components of SBs are HVAC and EWH. It can also be seen that SBs have RSP and BESS. Besides, SBs are equipped with smart metering and communication system that enables their direct connection with DSO and their participation in DRP. The figure also reflects that SBs have smart parking lots for charging/discharging residents' EVs. Lastly, it should mention that the gray nodes of the TS do not have a load.

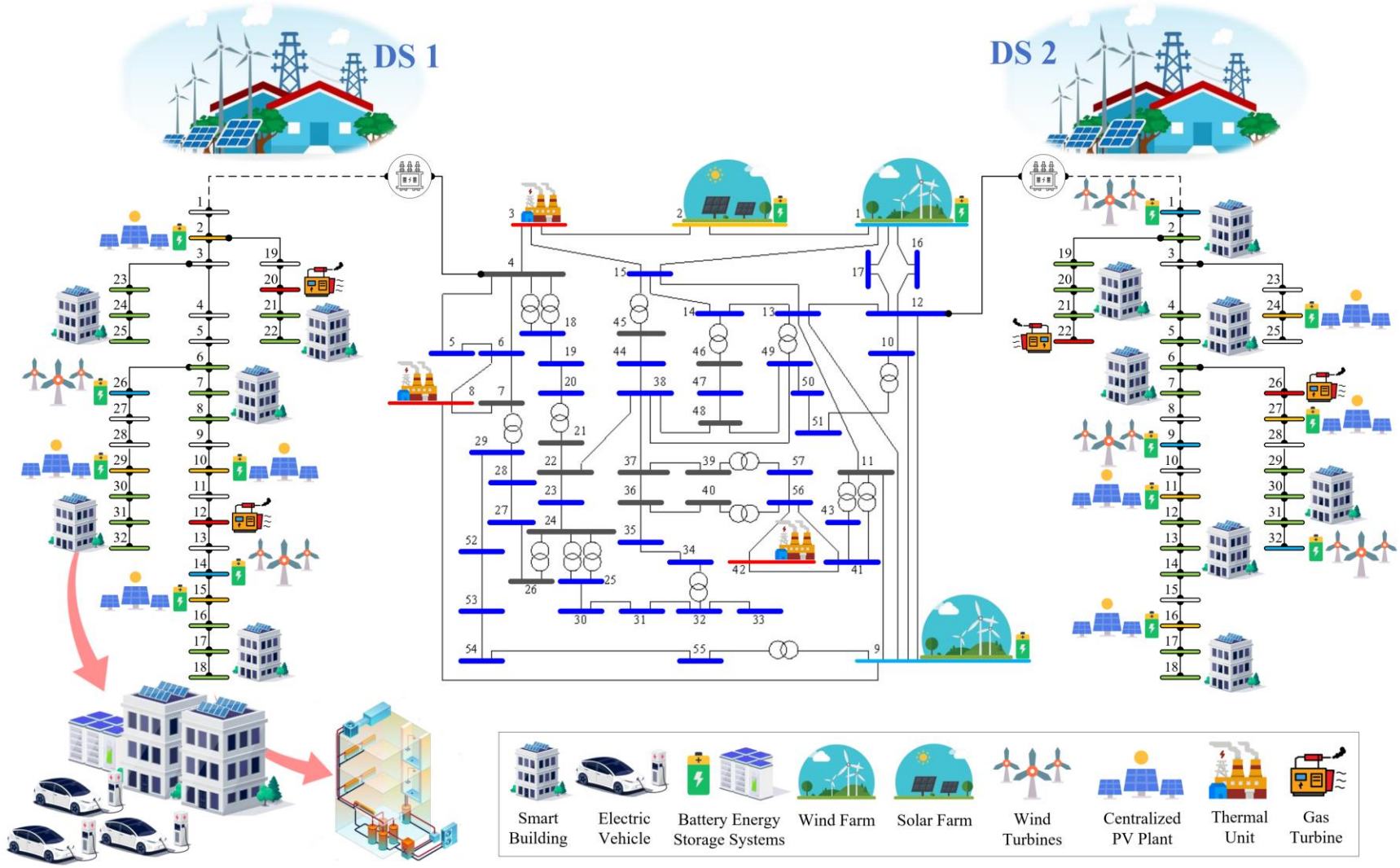

Fig. 3. The structure of the studied system

4.2. Input Data

Table 2 shows the design of different cases on which the proposed nested framework is implemented. As per this table, the impact of the two-stage interval-based optimization algorithm, distribution-wide DERs participation in the flexibility market and the proposed DRP design mechanism on the results will be evaluated in detail. In Tables 3-5, the information of network components, SBs and simulation parameters are respectively tabulated. The load demand curves of TS and DSs are shown in Figs. 4a-4c, while the TSO flexibility demand is shown in Fig. 4d. The load demand curve of SBs is depicted in Fig. 5a, while the ambient temperature is shown in Figs. 5b. Figure 5c demonstrates the hot water demand of the SB, based on which the EWH adjusts its operating point. Note that the desired indoor temperature of SBs is 24 degrees centigrade. Figure 5d depicts the 24-hour electricity price curve based on which SBs performs their DA scheduling. It is assumed that this curve is the average price of the last ten days. Finally, the curves of solar radiation and wind speed can be found in Figs. 6a and 6b, respectively.

Table 2. Structure of studied cases.

Case	Deterministic	Two-Stage Interval-Based Algorithm	Flexibility Options in Distribution-Wide		Implementing Proposed DRP Design Mechanism	
			DGs	BESSs	SBs	EV Fleets
1	✓	×	×	×	×	×
2	×	✓	×	×	×	×
3	×	✓	✓	×	×	×
4	×	✓	✓	✓	×	×
5	×	✓	✓	✓	✓	×
6	×	✓	✓	✓	✓	✓

Table 3. Information on components of TS and DSs

TS Components						
Components	**Location (Bus Number)**	**Capacity (MW)**	**Energy Price ($/MWh)**	**Flexibility Price ($/MWh)**	**Type**	
1	1	300	16	-	Wind Farm	
2	2	100	14	-	Solar Farm	
3	3	150	22	30	Thermal Unit	
4	8	60	25	34	Thermal Unit	
5	9	200	19	-	Wind Farm	
6	42	100	30	34	Thermal Unit	
DS Components						
Components	**Location (Bus Number)**	**Capacity (MW)**	**Energy Price ($/MWh)**	**Flexibility Price ($/MWh)**	**Type**	**Owner**
1	12	1.5	12	19	Gas Turbine	DS 1
2	20	1.5	14	16	Gas Turbine	DS 1
3	22	1.5	13	18	Gas Turbine	DS 2

4	26	1.5	11	17	Gas Turbine	DS 2
5	2	0.8	12	-	Centralized PV Plant	DS 1
6	10	1	10	-	Centralized PV Plant	DS 1
7	15	1	10	-	Centralized PV Plant	DS 1
8	29	0.8	11	-	Centralized PV Plant	DS 1
9	14	1	11	-	Wind Turbines	DS 1
10	26	1	12	-	Wind Turbines	DS 1
11	11	0.8	12	-	Centralized PV Plant	DS 2
12	16	1	11	-	Centralized PV Plant	DS 2
13	24	1	13	-	Centralized PV Plant	DS 2
14	27	0.8	11	-	Centralized PV Plant	DS 2
15	1	1	11	-	Wind Turbines	DS 2
16	9	2	12	-	Wind Turbines	DS 2
17	32	1	10	-	Wind Turbines	DS 2

Table 4. Information about the location and components of SBs

Smart Buildings	**Location (Bus Number)**	**Number of Consumers**	**RSP Capacity (kW)**	**Number of EVs**	**Owner**
1	6-7-8	420	300	180	DS 1
2	16-17-18	200	100	60	DS 1
3	21-22	150	100	60	DS 1
4	23-24-25	870	600	350	DS 1
5	30-31-32	500	300	150	DS 1
6	2	95	100	50	DS 2
7	4-5	170	150	70	DS 2
8	6-7	245	200	130	DS 2
9	12-13-14	220	150	100	DS 2
10	17-18	140	150	70	DS 2
11	19-20-21	250	150	110	DS 2
12	29-30-31	440	250	180	DS 2

Table 5. Information on simulation parameters

TS-DS Information						
Parameter	G^{STD}	$V^{\min}$	$V^{\max}$	η^{PV}	Δt	
Value (Unit)	1000 (W/m^2)	0.95 (p.u)	1.05 (p.u)	98 (%)	1 (h)	
BESSs Information						
Parameter	$\gamma^{Ch,\max}$	$\gamma^{Dis,\max}$	$SOC^{B,Initial}$	$SOC^{\min}$	$SOC^{\max}$	η^{Ch}	η^{Dis}
Value (Unit)	30 (%)	30 (%)	50 (%)	30 (%)	95 (%)	95 (%)	95 (%)
SBs Information							
Parameter	Δx	T^a / T^d	θ^{Cold}	$\theta^{B,Initial}$	$\theta^{W,Initial}$	v_{ci}	v_r
Value (Unit)	0.035 (m)	17:00 / 7:00 (h)	15 (C^o)	24 (C^o)	45 (C^o)	3 (m/s)	15 (m/s)
Parameter	v_{co}	α^B	α^{AC}	ω^B	ω^W	κ^B	κ^W
Value (Unit)	25 (m/s)	0.9	11 (C^o/MWh)	0.5	0.5	0.25	0.25

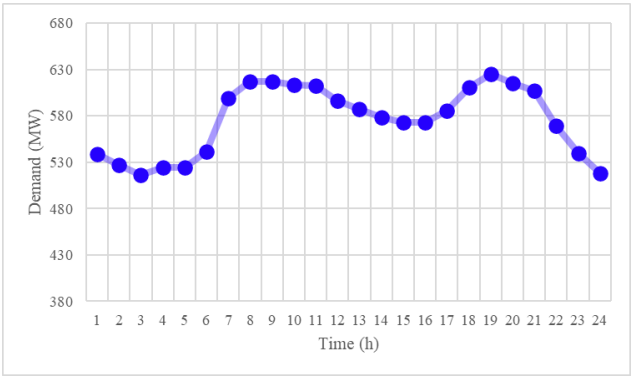

(a) Load demand of TS

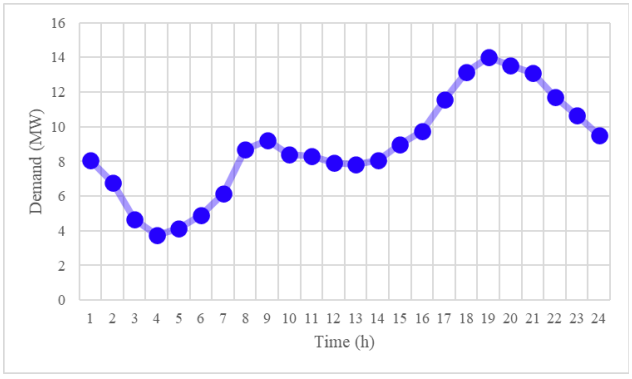

(b) Load demand of DS 1

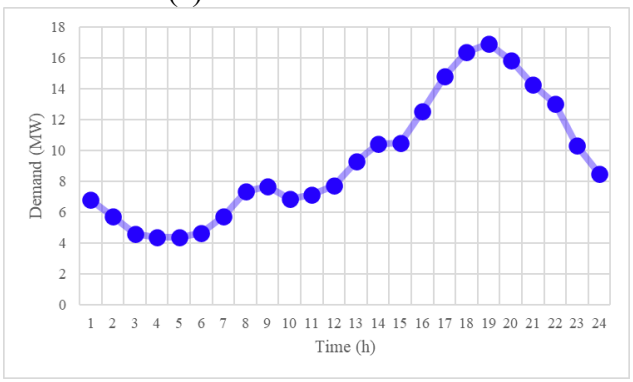

(c) Load demand of DS 2

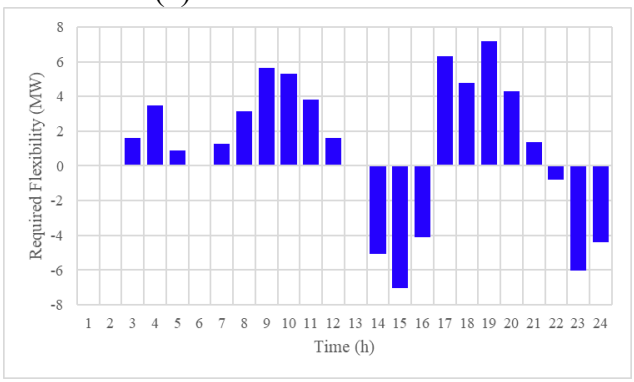

(d) Flexibility demand of TSO

Fig. 4. Load demand curves of TS and DSs

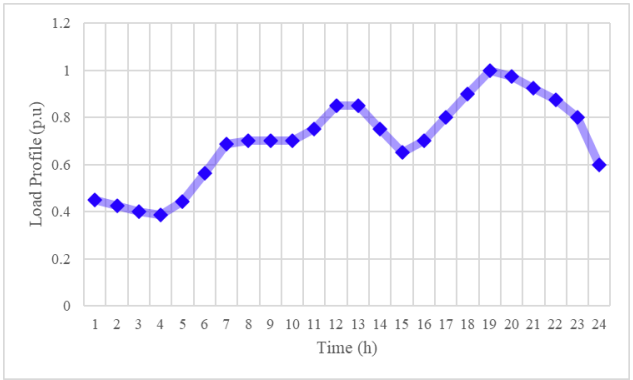

(a) Load demand curve of SBs

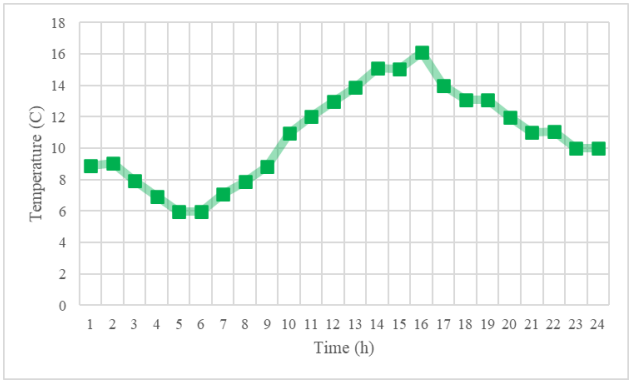

(b) Ambient temperature

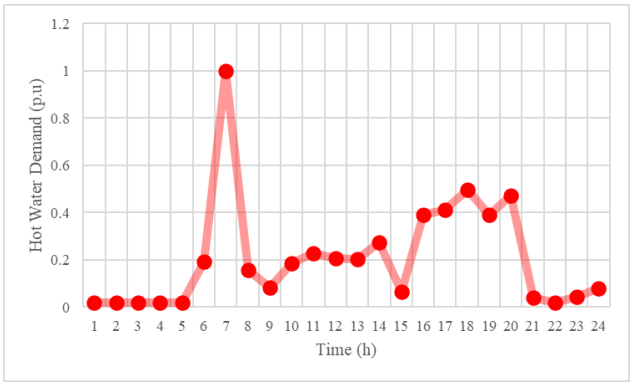

(c) Hot water demand curve of SBs

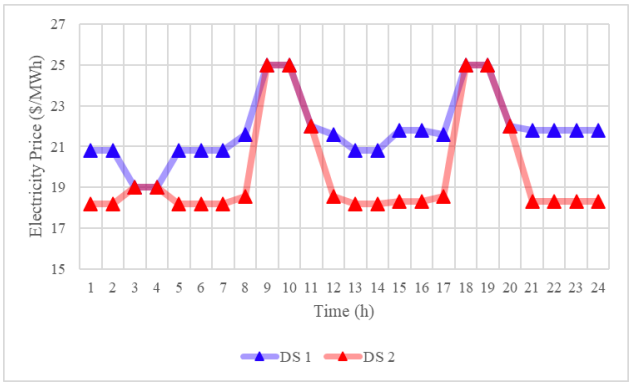

(d) The average electricity price of the previous 10 days

Fig. 5. Input parameters needed to model SBs

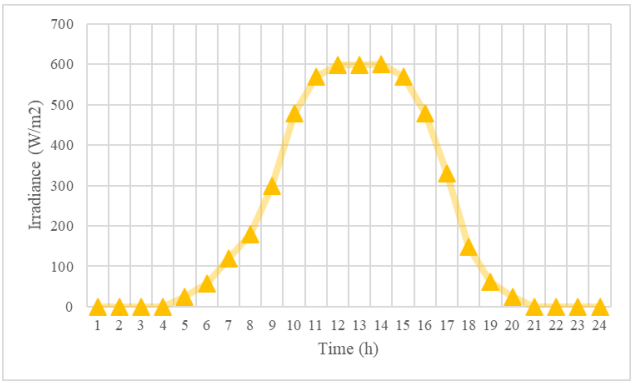

(a) Solar radiation

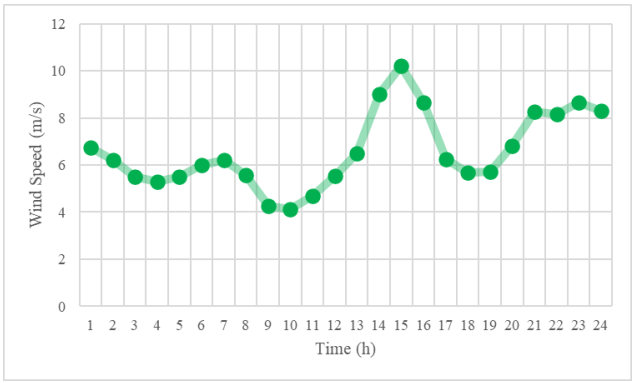

(b) Wind speed

Fig. 6. Curves of solar radiation and wind speed

4.3. Results of Case 1 (C1) and Case 2 (C2)

C1 and C2 are designed to investigate the effect of the two-stage interval-based optimization algorithm on the operation results. In C1, the proposed nested framework is solved in deterministic mode, while in C2 it is solved via the proposed two-stage interval-based optimization algorithm. Tables 6 and 7, respectively, tabulate the numerical results of C1 and C2. As per these tables, the application of the two-stage interval-based technique in C2 has relatively increased the operating costs of TS and DSs compared to C1, which is due to the determination of an interval for each uncertain parameter and performing the operational planning with a pessimistic viewpoint. Note that the values of uncertain parameters in the proposed two-stage interval-based technique are determined after solving an iteration-based process.

Figures 7a-7e show the curves obtained for uncertain parameters in C2 where the interval of each parameter is also shown. These figures reveal that the obtained curves for all parameters in C2 have worse conditions compared to C1 (deterministic mode), so that the wind speed and solar radiation are lower while the load demand is higher. On the other hand, the comparison of the curves obtained for uncertain parameters in C2 with their upper and lower levels shows that the worst condition is not considered for any of them, which is an important point to keep the planning within the optimal range.

As mentioned, in the proposed two-stage interval-based technique, BESSs are responsible for covering extreme conditions, where their operating point is determined according to the worst-case scenario. In this light, Figs. 8a-8d are presented to analyze the performance of BESSs, before and after the implementation of the proposed two-stage interval-based technique. In these figures, the operating points obtained for BESSs in stages 1 and 2 are compared. As can be seen, considering extreme conditions in stage 2 has changed the operating points of BESSs almost throughout the operation period compared to stage 1. Figure 9 is provided to study the impact of uncertainties on the hourly cost of the system, where the daily costs obtained in deterministic, proposed two-stage interval-based technique, pessimistic and optimistic modes are compared. As per this figure, the lowest and highest costs are respectively for optimistic and pessimistic modes. It can also be observed that the system cost in the interval-based mode is between deterministic and pessimistic curves, which is due to our pessimistic-oriented planning.

Table 6. Numerical results obtained from the implementation of C1

Entity	**Operation Costs ($)**				**Trading with Customers ($)**		
	Fee Paid to Components	**Exchange in Coupling Node**		**Sum**	**Bounous Paid for DRP**	**SBs**	**RLs**
		Energy	**Flexibility**				
TS	264727.89	-3157.90	0	261569.99	-	-	321939.72
DS 1	1357.68	1789.29	0	3146.9734	0	2931.62	1908.81
DS 2	1540.29	1368.61	0	2908.8993	0	2122.03	2598.53
Total	267625.86				331500.72		

Table 7. Numerical results obtained from the implementation of C2

Entity	Operation Costs ($)				Trading with Customers ($)		
	Fee Paid to Components	Exchange in Coupling Node		Sum	Bounous Paid for DRP	SBs	RLs
		Energy	Flexibility				
TS	277515.86	-3520.29	0	273995.56	-	-	335139.25
DS 1	1315.52	1967.00	0	3282.5132	0	3045.96	1985.16
DS 2	1491.05	1553.30	0	3044.347	0	2205.85	2702.47
Total	280322.42				345078.70		

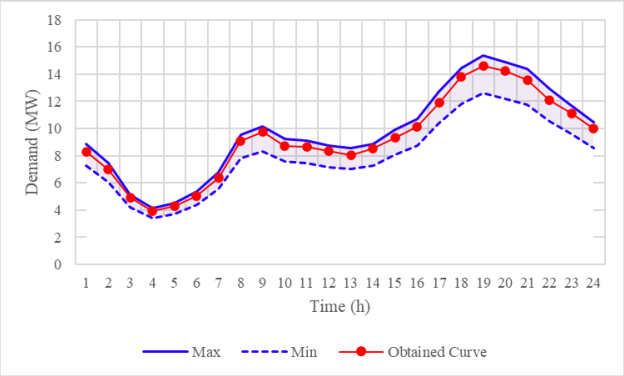

(a) Load demand of DS 1

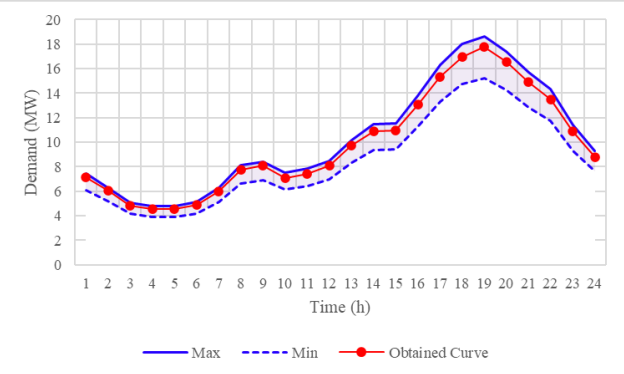

(b) Load demand of DS 2

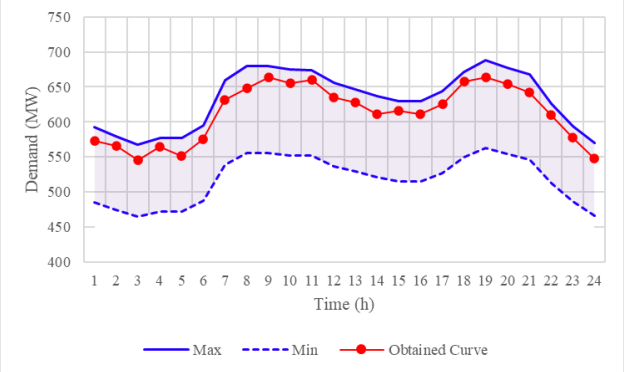

(c) Load demand of TS

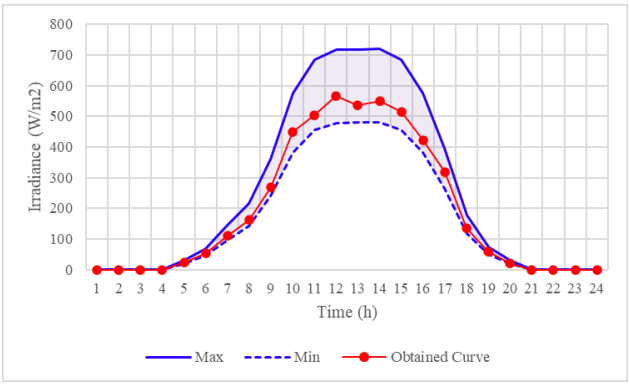

(d) Solar radiation

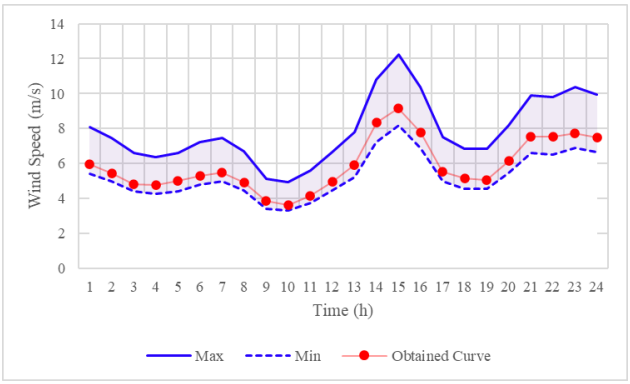

(e) Wind speed

Fig. 7. Daily curves of the uncertain parameters in C1 & C2

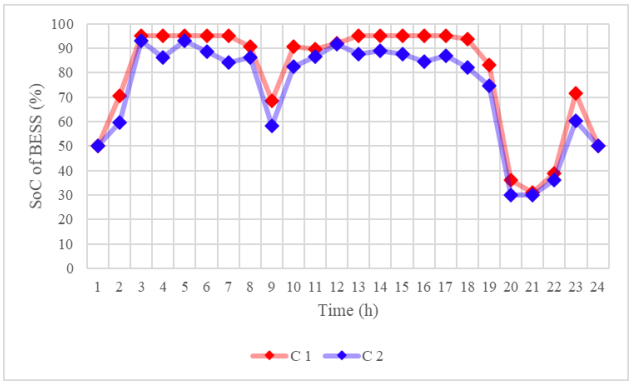

(a) BESS placed on node 10 of DS 1

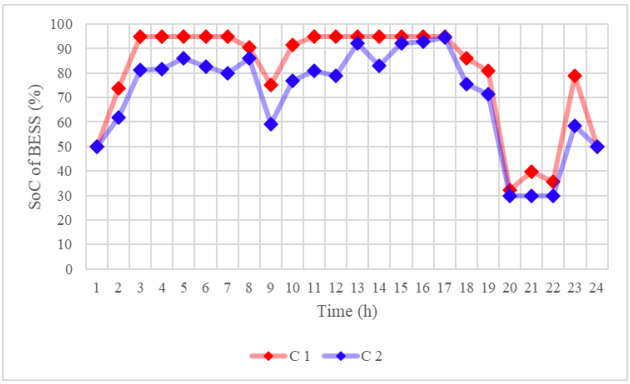

(b) BESS placed on node 26 of DS 1

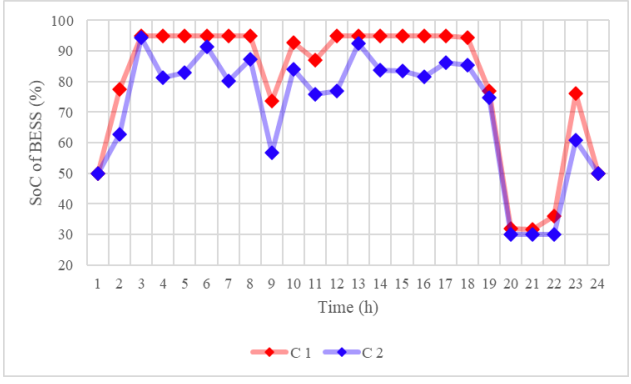

(c) BESS placed on node 1 of TS

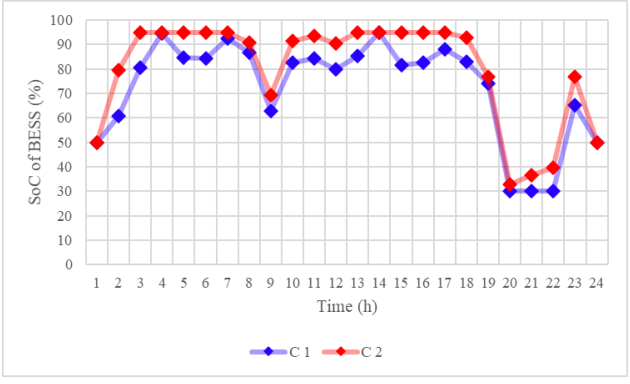

(d) BESS placed on node 2 of TS

Fig. 8. Comparison of BESSs operating point in C1 & C2

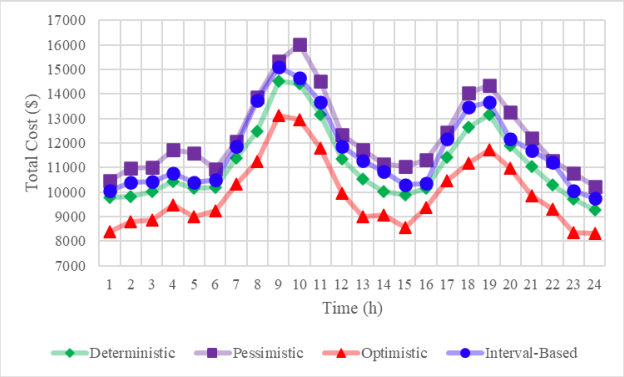

Fig. 9. Total hourly costs of the system in different modes

4.4. Results of Case 3 (C3) and Case 4 (C4)

C3 and C4 are designed to investigate the impact of distribution-wide DERs participation in the flexibility market on the technical and economic aspects of the system. The results presented in Tables 8 and 9 reveal that the total daily costs of the system in C3 and C4 have decreased by 410.33 $ and 611.57 $, respectively, over C2, which is due to the provision of part of the upward and downward flexibility capacities through distribution-wide DERs instead of expensive transmission-wide TUs. Figures 10a and 10b illustrate the contribution of system components in providing flexibility capacities in C3 and C4, respectively. As per these figures, GTs and BESSs of the DSs have a considerable contribution in providing upward and downward flexibility capacities. Figures 10a and 10b also demonstrate that the rest of the flexibility capacities are provided through TUs, and BESSs of the transmission system.

The analysis of the numbers in Tables 8 and 9 clarify that the participation of distribution-wide DERs in the flexibility market brings profits of $969.56 and $1147.59 to the DSs in C3 and C4, respectively. On the other hand, the results reveal that the costs of DSOs in the energy market in C3 and C4 increased by 1.61% and 1.67%, respectively, compared to C2, which is due to the allocation of a significant part of the their DERs to the flexibility market and as a result their less participation in the energy market. However, total system costs have decreased in C3 and C4 compared to C2, because the reduction in flexibility market costs has been greater than the increase in energy market costs.

Figures 11a-11d, respectively, depict the LMP and FLMP of coupling points in C2 to C4. Figures 11a and 11b reflect that the LMP level of the coupling points in C2 is lower than C3 and C4, which is due to the purchase of more power by DSs. In contrast, Figs. 11c and 11d reveal that the participation of DERs in the flexibility market has significantly reduced the FLMP at the coupling points.

Table 8. Numerical results obtained from the implementation of C3

Entity	Operation Costs ($)				Trading with Customers ($)		
	Fee Paid to Components	Exchange in Coupling Node		Sum	Bounous Paid for DRP	SBs	RLs
		Energy	Flexibility				
TS	276586.36	-3577.19	969.56	273978.73	-	-	342177.18
DS 1	1556.58	2044.84	-528.56	3072.8695	0	3112.97	2024.87
DS 2	1769.14	1532.35	-441.01	2860.4877	0	2249.97	2759.23
Total	279912.08				352324.21		

Table 9. Numerical results obtained from the implementation of C4

Entity	Operation Costs ($)				Trading with Customers ($)		
	Fee Paid to Components	Exchange in Coupling Node		Sum	Bounous Paid for DRP	SBs	RLs
		Energy	Flexibility				
TS	276412.14	-3579.31	1147.59	273980.42	-	-	347309.84
DS 1	1557.30	2035.52	-608.28	2984.53	0	3162.77	2059.29
DS 2	1741.41	1543.79	-539.30	2745.90	0	2290.47	2806.13
Total	279710.85				357628.50		

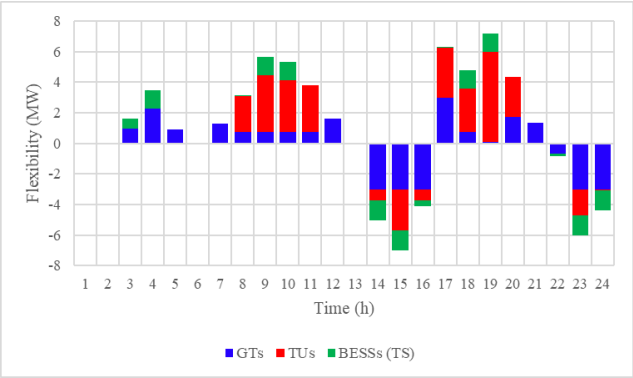

(a) Flexibility providers in C3

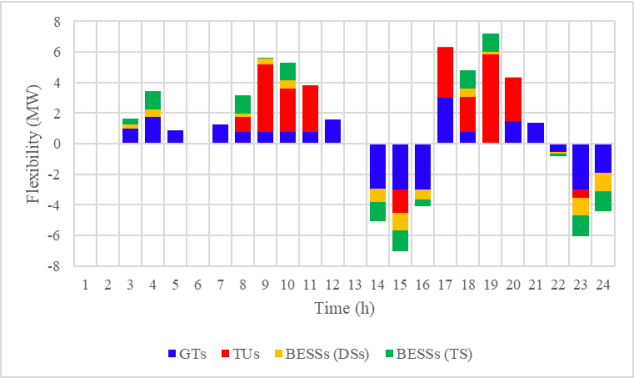

(b) Flexibility providers in C4

Fig. 10. The contribution of components in providing flexibility capacities in C3 & C4

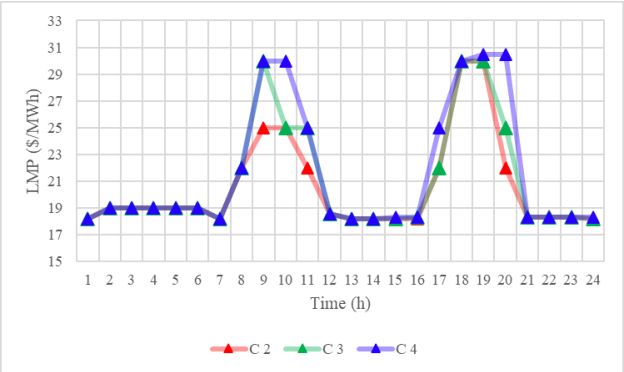

(a) LMP at coupling point of TS and DS 1

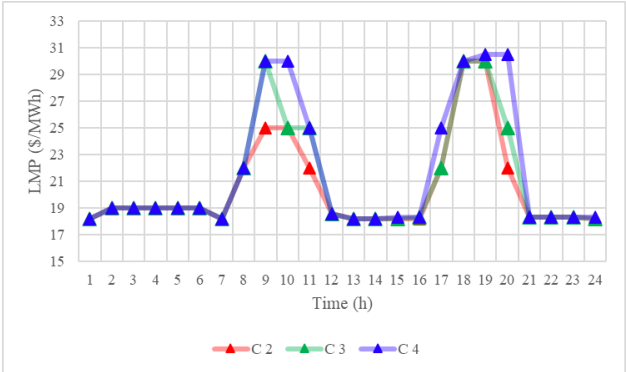

(b) LMP at coupling point of TS and DS 2

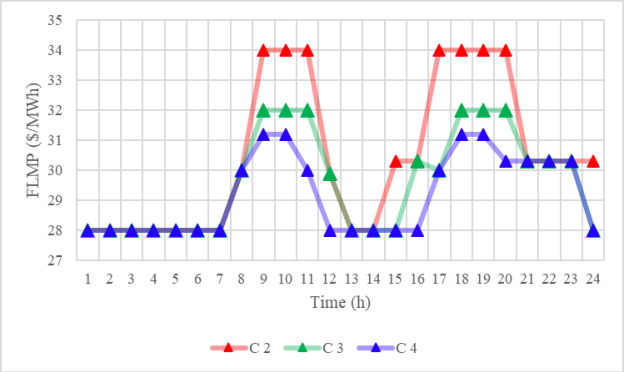

(c) FLMP at coupling point of TS and DS 1

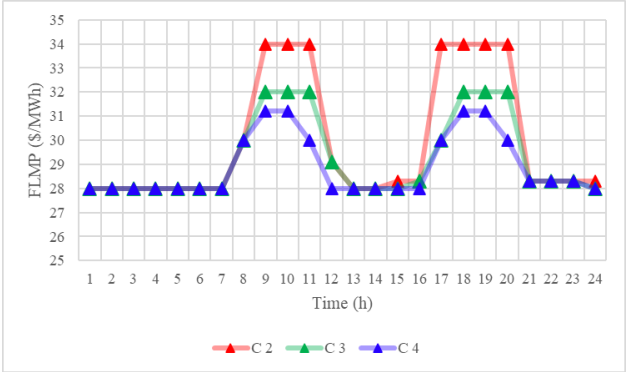

(d) FLMP at coupling point of TS and DS 2

Fig. 11. LMP and FLMP of coupling points in C2 to C4

4.5. Results of Case 5 (C5) and Case 6 (C6)

In C5 and C6, the impact of the behavior of SBs and EV fleets on the technical and economic factors of the system is studied in detail. In this light, we have presented a new mechanism for designing DRP tariffs with time-varying incentives to take advantage of SBs and EV fleets to deal with flexibility challenges. In C5, this mechanism is implemented where the EMSs of SBs perform the operating point of their controllable components including HVAC, EWH and BESS based on time-varying incentive tariffs. The results of Table 10 testifies that the implementation of the proposed DRP design mechanism in C5 not only reduces the costs of DSOs in the energy market by 9.17%, but also increases their profit by 23.74%. In addition, the numerical results clarify that the implementation of the proposed DRP design mechanism in C5 has reduced the daily costs of TSO by 80.14 $.

Figure 12 provides the incentive tariffs designed by the proposed DRP mechanism. As you can see, the rewards are time-varying, and their amount alternates based on the flexibility demand of TSO. The effect

of implementing the proposed DRP design mechanism on the operating point of the controllable components of a SB is analyzed through Figs. 13a-13c. According to Figures 13a and 13b, after implementing the proposed DRP design mechanism, the EMS of building has changed the operating points of HVAC, EWH and BESS where they are in line with the upward and downward flexibility requirements of the system. It is clear from Figs. 13a and 13b that the implementation of the proposed DRP design mechanism lowers the operating points of HVAC and EWH during high-demand periods. Figure 13c shows that the BESS placed in the SB in C4 is operated according to the energy market price, so that it is charged in cheap hours and discharged in expensive hours. On the other hand, it can be seen that the provision of incentive tariffs to the SB has changed the pattern of BESS operation in C5, so that it is fully in line with system flexibility requirements. The performance of controllable components shows that the proposed DRP design mechanism is able to use the potential of SBs to improve the technical aspects of the system while reducing the operating costs.

Figures 14a and 14b indicate the indoor temperature and the EWH's output water temperature of a SB in C4 and C5. Figure 14a illustrates that the indoor temperature of the building deviated by about 1.5 degrees from the residents' desired temperature in two periods, which is due to the participation of the building in DRP. Similarly, Fig. 14b shows the deviation of the outlet water temperature from the desired temperature of the residents in some periods. Examining these figures reveals that the EMS of the SB has not exceeded the permitted thermal comfort range despite the deviation from the residents' desired temperature.

In Figs. 15a and 15b, the effect of implementing the proposed DRP design mechanism on the system voltage is investigated. These figures clear that the average magnitude of the voltage of DSs during the entire operation period in C5 was at a higher level than C4, which leads to the improvement of operation security. Figures 16a-16f indicate the effect of the proposed DRP design mechanism on the congestion of TS and DSs. These figures are plotted for 19:00 o'clock (Peak hour). As can be seen form Figs. 16a-16f, the power flow level of most lines of the DSs in C5 has decreased compared to C5, which is due to the significant reduction in the load of SBs in peak hour. On the other hand, the analysis of Figs. 16e and 16f

shows that the congestion in lines 11, 19, 20 and 23 of the TS has been relieved in C5 compare to C4, which is due to the reduction of the load of DSs 1 and 2 in peak hour. It should be noted that in Figs. 16e and 16f, only the lines whose capacity is filled more than 70% were plotted.

Figures 17a-17d depict the LMP and FLMP obtained for the coupling points at C4 and C5. As you can see, the LMP and FLMP curves in C5 have not only decreased significantly in high-demand periods, but also become smoother. These curves prove that through the implementation of an effective DRP mechanism, it is possible to reduce the clearing price of energy and flexibility markets in high-demand periods. Note that the reason for the reduction of FLMP is the supply of a larger part of the system flexibility demand by distribution-wide DERs in C5 compare to C4.

Figure 18 compares the flexibility capacities provided by distribution-wide DERs in C4 and C5, according to which DERs have provided more flexibility in C5 than C4. Note that with the implementation of the proposed DRP design mechanism in C5, the load demand of SBs has decreased during peak periods of the upward flexibility market, which has led to the allocation of a larger portion of DERs capacity to this market. On the other hand, DRP implementation has increased the load demand of SBs during the peak periods of the downward flexibility market, which has led to a higher operating point of DERs and subsequently more participation in the downward flexibility market.

Table 10. Numerical results obtained from the implementation of C5

Entity	**Operation Costs ($)**				**Trading with Customers ($)**		
	Fee Paid to Components	**Exchange in Coupling Node**		**Sum**			
		Energy	**Flexibility**		**Bounous Paid for DRP**	**SBs**	**RLs**
TS	275731.24	-3251.03	1420.07	273900.29	-	-	337932.47
DS 1	1607.08	1867.10	-813.59	2660.59	270.01	2706.37	2003.69
DS 2	1750.37	1383.93	-606.49	2527.81	216.90	2050.02	2730.37
Total	279088.69				346935.99		

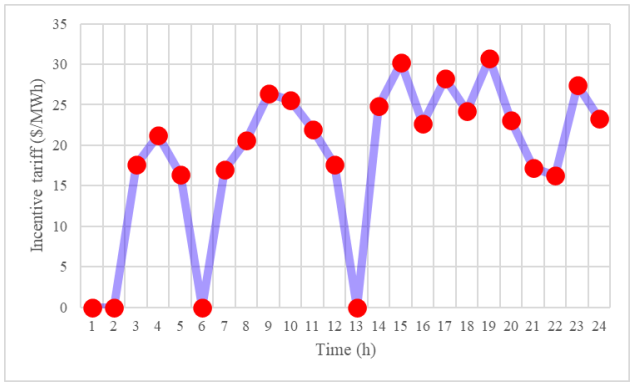

Fig. 12. Incentive tariffs built by the proposed DRP design mechanism

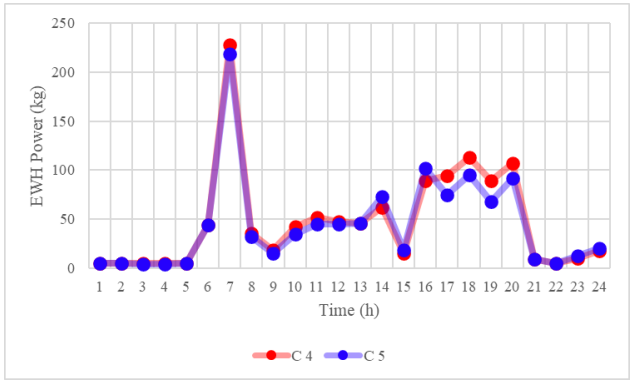

(a) HVAC

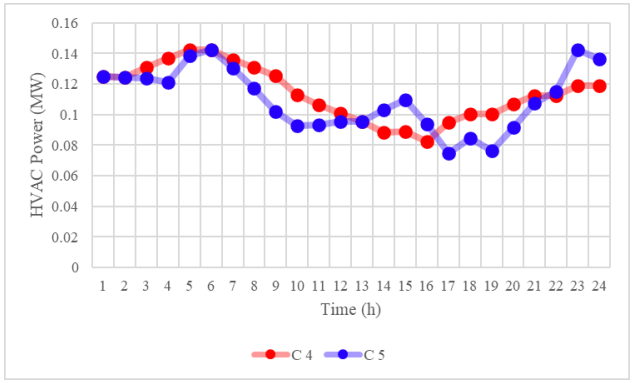

(b) EWH

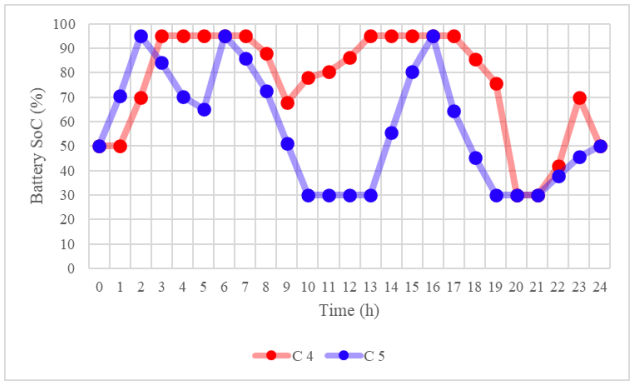

(c) BESS

Fig. 13. The operating point of controllable components of the SB placed on bus 2 in DS 2: C4 & C5

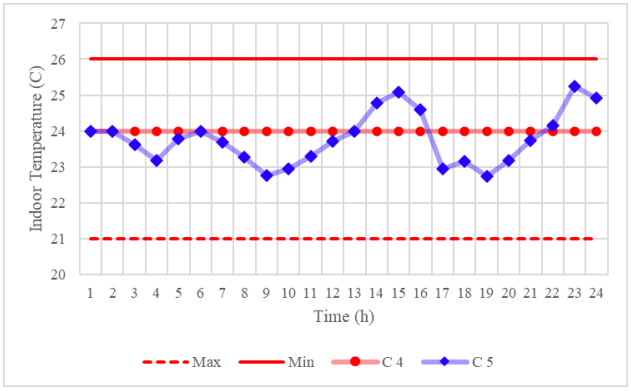

(a) Indoor temperature

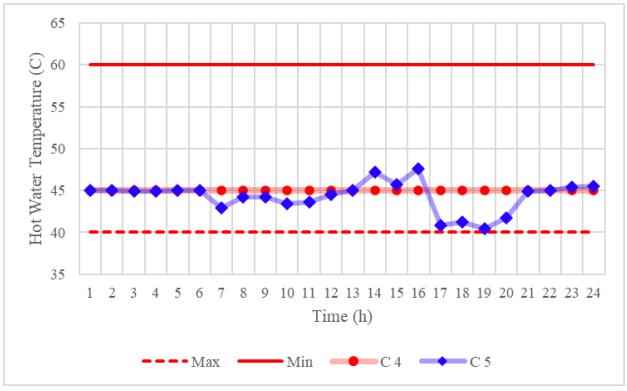

(b) EWH's output water temperature

Fig. 14. Indoor temperature and EWH's output water temperature of a SB in C4 & C5

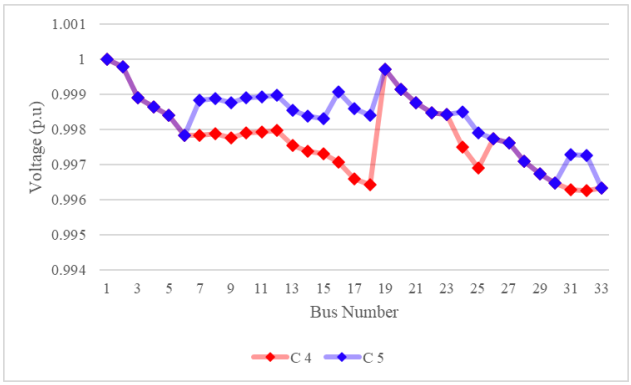

(a) Average voltage magnitude of DS 1

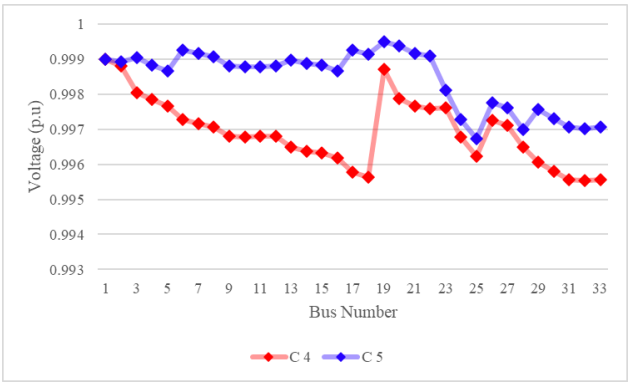

(b) Average voltage magnitude of DS 2

Fig. 15. The average voltage of DSs 1 and 2 during the operation period in C4 & C5

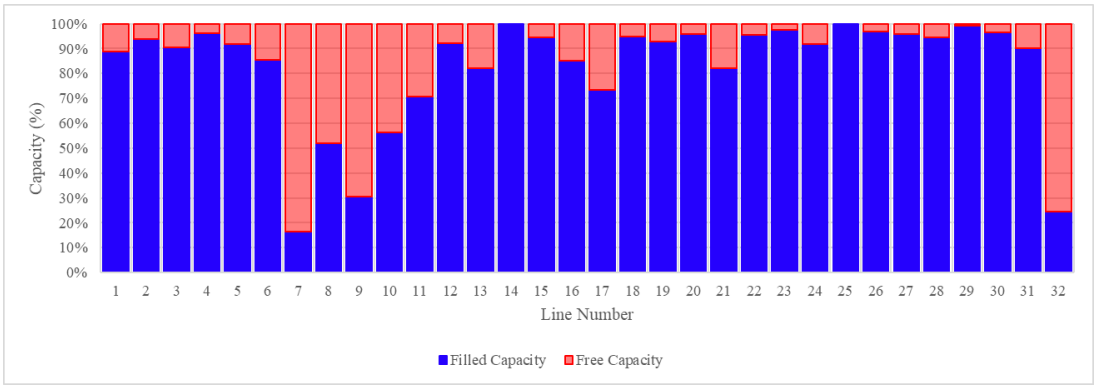

(a) DS 1 in C4

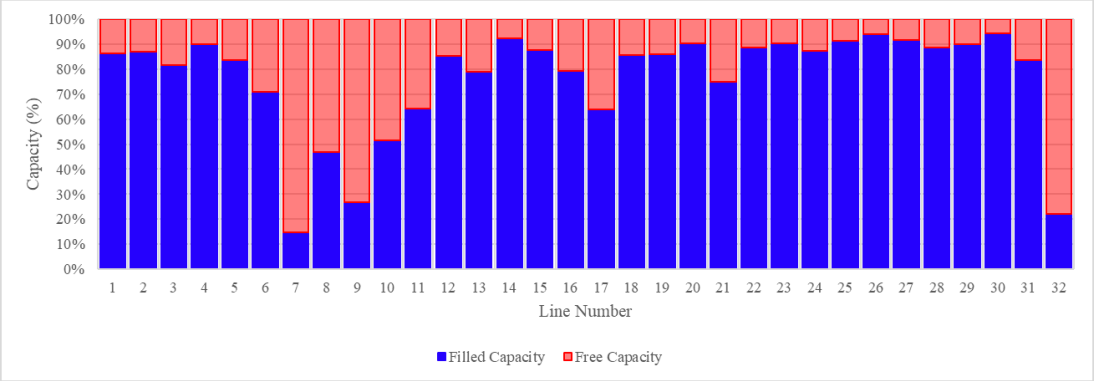

(b) DS 1 in C5

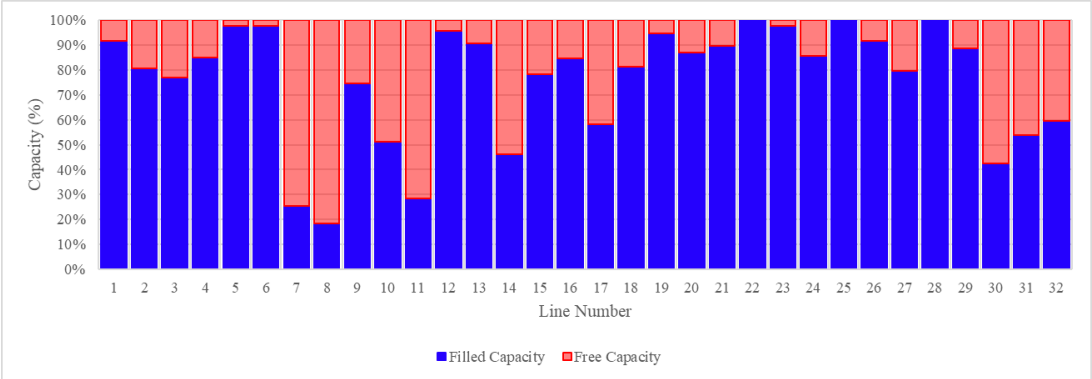

(c) DS 2 in C4

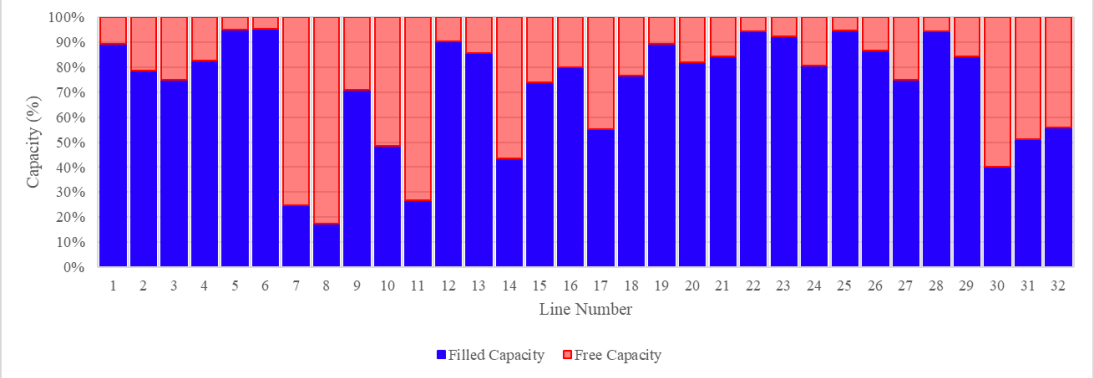

(d) DS 2 in C5

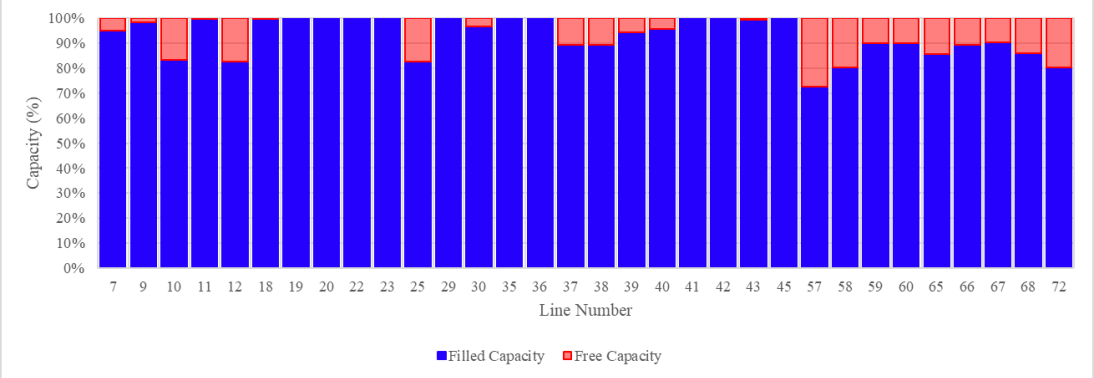

(e) TS in C4

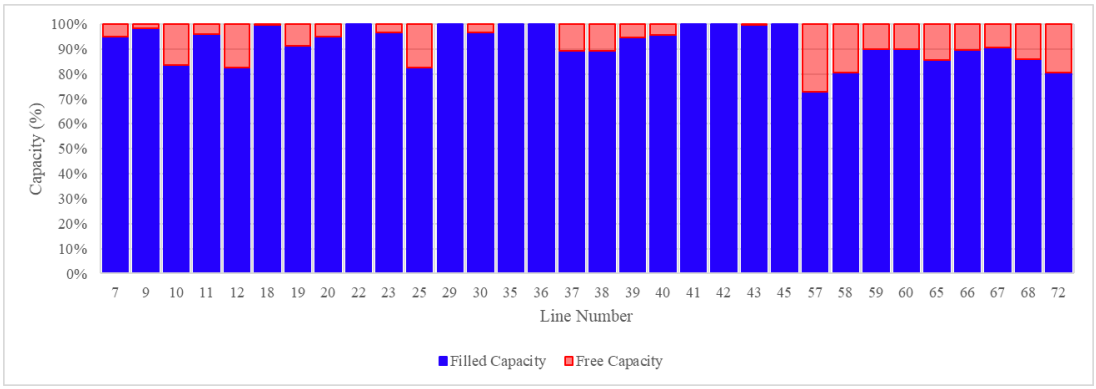

(f) TS in C5

Fig. 16. The used capacity of the lines at 19:00 in C4 & C5

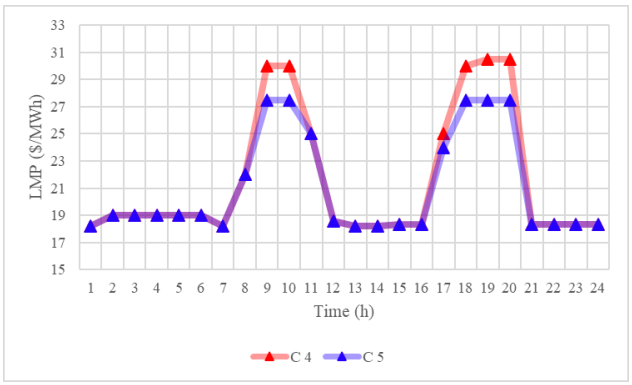

(a) LMP at coupling point of TS and DS 1

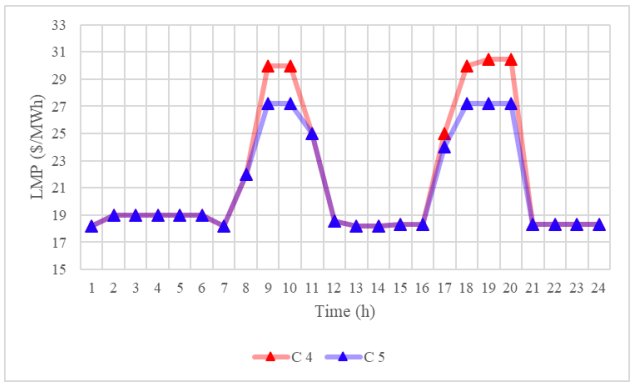

(b) LMP at coupling point of TS and DS 2

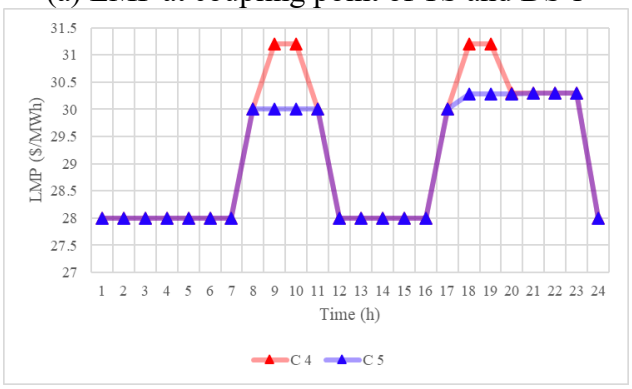

(c) FLMP at coupling point of TS and DS 1

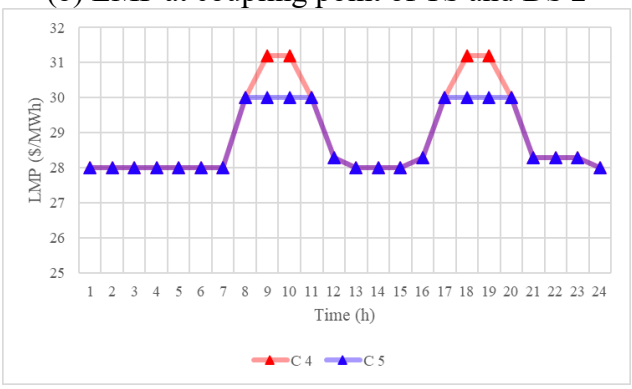

(d) FLMP at coupling point of TS and DS 2

Fig. 17. LMP and FLMP of coupling points in C4 & C5

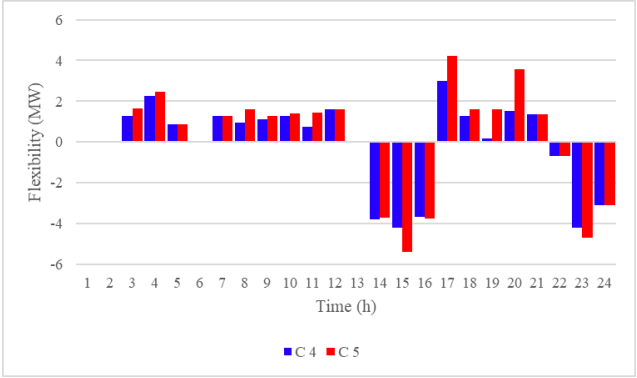

Fig. 18. Comparison of flexibility capacities provided by DSs in C4 & C5

Table 11 presents the results of C5 where the EV fleet also participates in the proposed DRP. From the analysis of the results in Table 11, it can be found that the participation of EVs in DRP has lowered the costs of SBs, and energy and flexibility markets as well. It should be mentioned that these EVs belong to the residents of SBs and are charged / discharged in the parking lot of the building. Figures 19a and 19b compare the scheduling of EV fleets in C5 and C6. The analysis of the curves reveals that the participation of EV fleets in DRP aligns their schedules with network requirements so that they are discharged during the peak periods of energy and upward flexibility markets, while they are charged during the off-peak period of downward flexibility market. This performance has a positive effect on the LMP and FLMP at the coupling points, as shown in Figures 20a-20d. These figures reveal that the provision of V2G services by EV fleets not only smoothed the LMP and FLMP curves, but also lowered their levels in high-demand periods. Figure 21 is presented to analyze the impact of V2G services on network congestion, where the filled capacity of lines of the system in C5 and C6 are compared. This comparison illustrates that the provision of V2G services not only reduced the filled capacity of lines in DSs 1 and 2, but also reduced the congestion of lines 11, 19, 20 and 23 of the TS. Overall, the results testify that the provision of V2G services along with the participation of SBs in DRP has positive effects on voltage profile, lines' congestion and system operating costs.

Table 11. Numerical results obtained from the implementation of C6

Entity	**Operation Costs ($)**				**Trading with Customers ($)**		
	Fee Paid to Components	**Exchange in Coupling Node**		**Sum**	**Bounous Paid for DRP**	**SBs**	**RLs**
		Energy	**Flexibility**				
TS	275351.15	-2963.45	1450.31	273838.00	-	-	331849.69
DS 1	1589.24	1697.42	-785.99	2500.66	450.02	2489.86	1967.62
DS 2	1776.74	1266.03	-664.32	2378.46	361.51	1886.02	2681.22
Total	278717.12				340062.87		

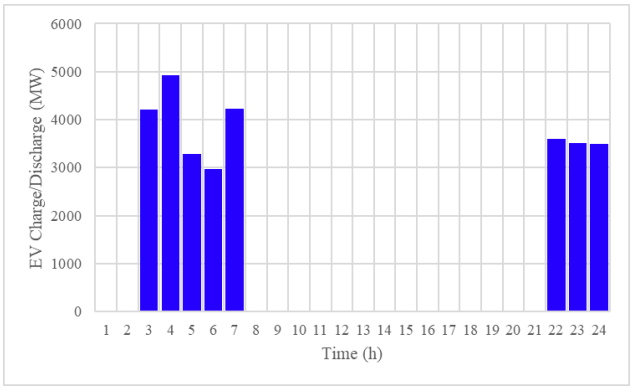

(a) EV fleets in C5

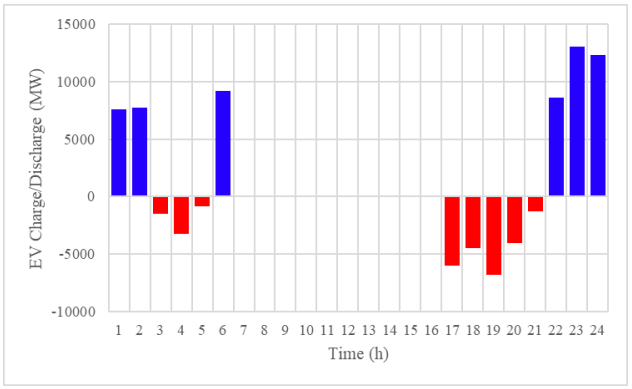

(b) EV fleets in C6

Fig. 19. Schedules of EV fleets in C5 and C6

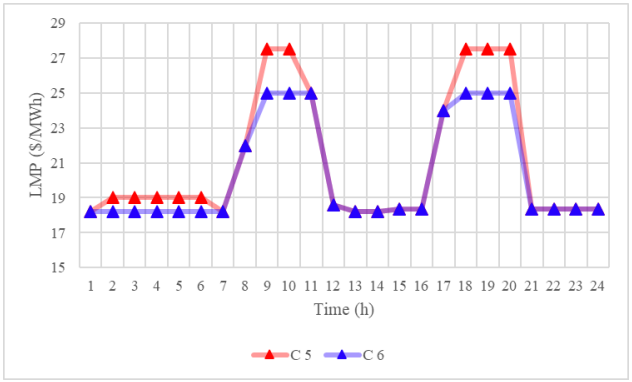

(a) LMP at coupling point of TS and DS 1

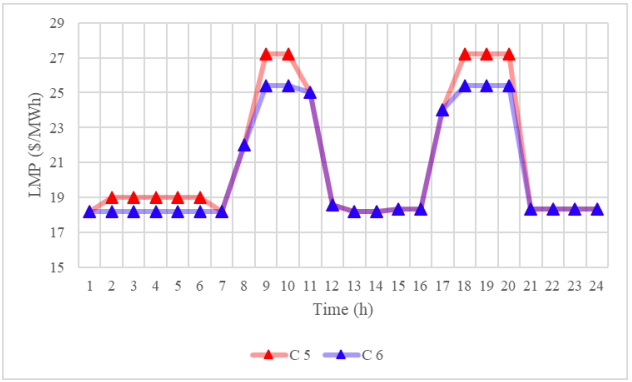

(b) LMP at coupling point of TS and DS 2

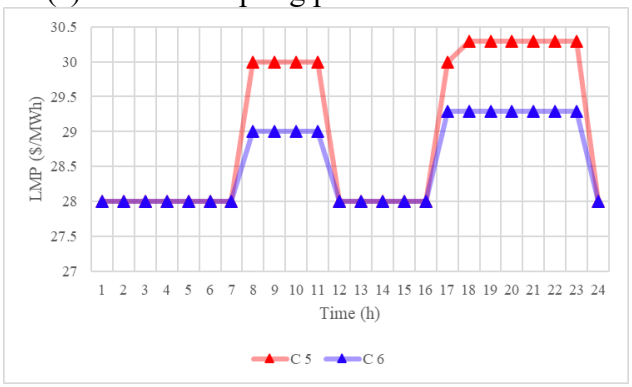

(c) FLMP at coupling point of TS and DS 1

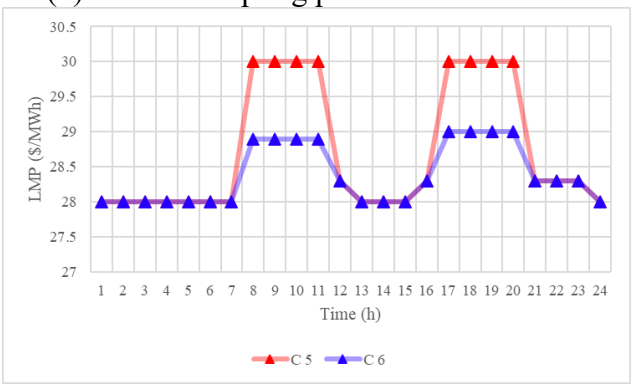

(d) FLMP at coupling point of TS and DS 2

Fig. 20. LMP and FLMP of coupling points in C5 & C6

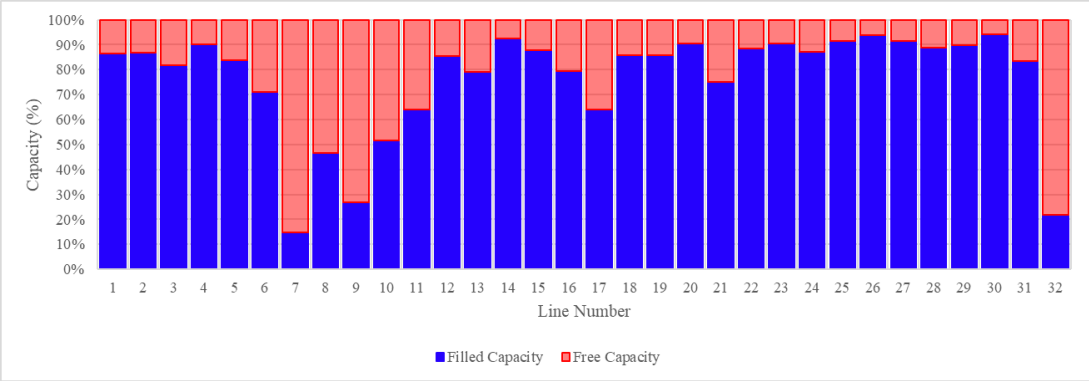

(a) DS 1 in C5

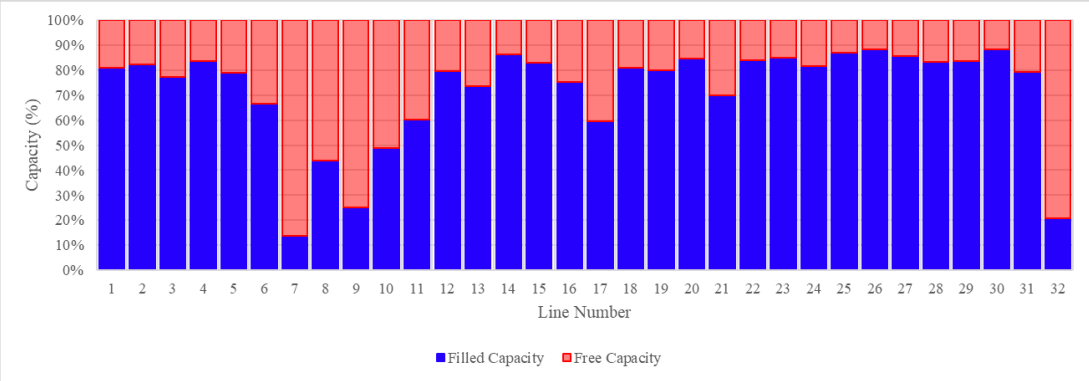

(b) DS 1 in C6

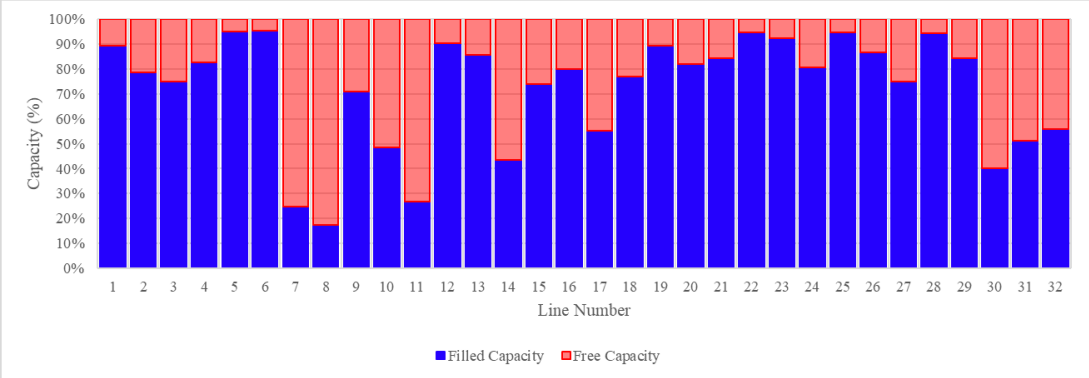

(c) DS 2 in C5

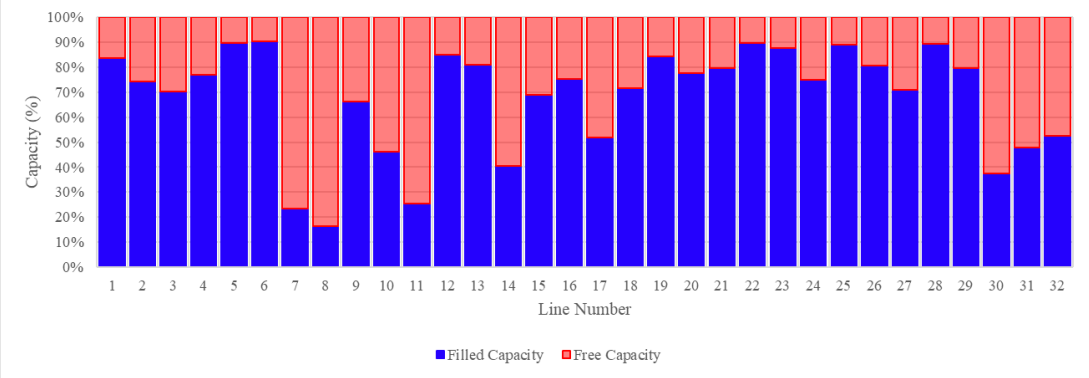

(d) DS 2 in C6

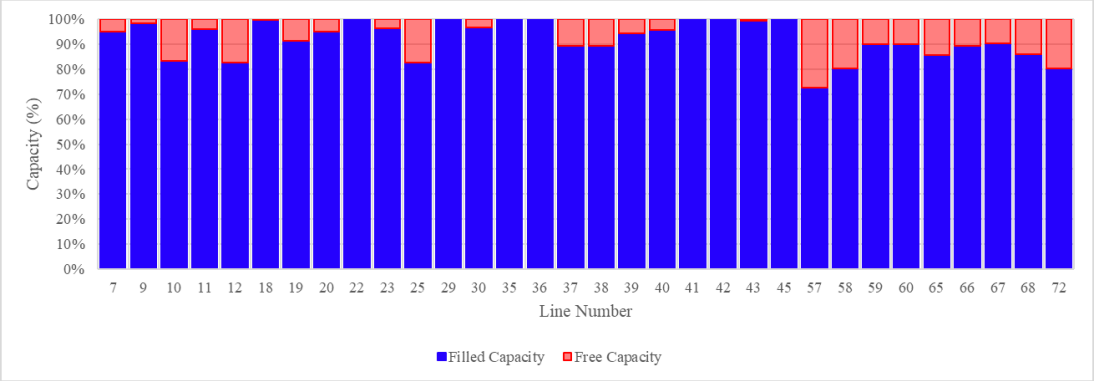

(e) TS in C5

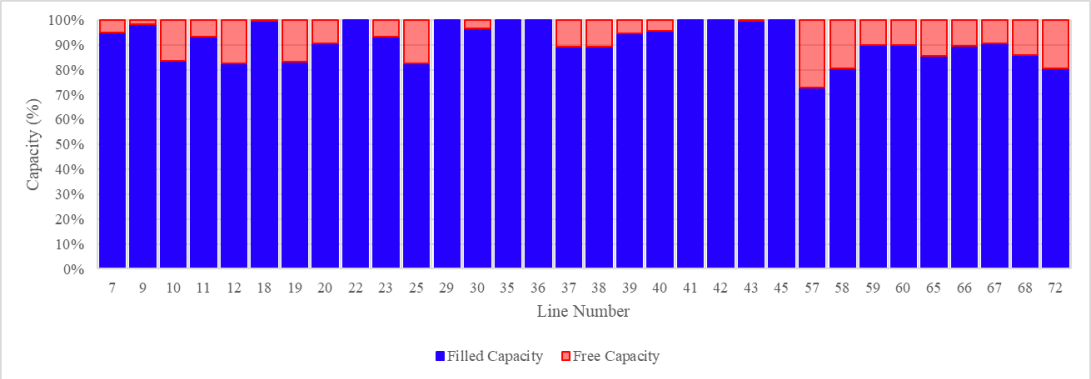

(f) TS in C6

Fig. 21. The used capacity of the lines at 19:00 in C5 & C6

5. Conclusion

In this work, a nested framework for TSO-DSO coordination under the influence of a high number of RGs was presented, taking into account the active participation of SBs and EV fleets in scheduling. Moreover, a time-varying DRP design mechanism was introduced to align the scheduling of SBs and EV fleets with flexibility requirements of the system. The coordination of TSO and DSO was initially modeled as a NLP bi-level problem, and then it was transformed into a single-level MPEC problem using KKT conditions, Big-M method, and SDT. The impact of the proposed nested framework on the economic, technical and security aspects of the system was evaluated through the implementation of several case studies, the important results of which are as follows:

- A two-stage interval-based algorithm was used to deal with uncertainties. The results testified that the proposed algorithm determined the operating points of BESSs with the aim of ensuring safe operation during extreme conditions. Analysis of the numerical results revealed that the interval-

based technique, despite the 4.74% increase in total costs, determined a safe interval for the fluctuation of the parameters, which increased the security of operation.

- The results showed that providing the flexibility required by TSO through the distribution-wide DERs including GTs and BESSs instead of transmission-wide TUs, reduced the total daily costs of DSs by 3.84%.
- The results of the implementation of the proposed DRP design mechanism confirmed that this mechanism aligned the schedules of SBs and EV fleets with the flexibility requirements of the system. The results showed that the proposed DRP mechanism, by motivating SBs and EV fleets to change their scheduling, reduced LMP and FLMP at coupling points. The numerical results mirrored that the implementation of the proposed DRP mechanism not only reduced the costs of DSOs in the energy market by 9.17%, but also increased their profit from participating in the flexibility market by 23.74%.
- The simulation results also proved that changing the operating point of thermostatically-controllable loads and BESSs along with providing V2G services through the implementation of the proposed DRP design mechanism, released a significant part of the capacity of distribution-wide DERs in high-demand periods and subsequently increased their contribution in the flexibility market. Moreover, the results testified that the peak-shaving resulting from the implementation of the proposed DRP mechanism not only reduced the congestion in TS and DS lines, but also improved the voltage profile.

Overall, the results clarified that the proposed interval-based nested framework, which is computationally tractable by linear solvers such as CPLEX, GUROBI, etc., was able to improve the technical, economic and security aspects of coordinated TSO-DSO operational planning by utilizing the potential of SBs and EV fleets through a powerful DRP design mechanism.

Acknowledgment

This work is supported by DTE Network+ funded by EPSRC grant reference EP/S032053/1.

References

[1] Nastasi B, Markovska N, Puksec T, Duić N, Foley A. Renewable and sustainable energy challenges to face for the achievement of Sustainable Development Goals. Renew Sustain Energy Rev 2022;157:112071. https://doi.org/https://doi.org/10.1016/j.rser.2022.112071.

[2] Sebestyén V. Renewable and Sustainable Energy Reviews: Environmental impact networks of renewable energy power plants. Renew Sustain Energy Rev 2021;151:111626. https://doi.org/https://doi.org/10.1016/j.rser.2021.111626.

[3] Li Y, Taghizadeh-Hesary F. The economic feasibility of green hydrogen and fuel cell electric vehicles for road transport in China. Energy Policy 2022;160:112703. https://doi.org/https://doi.org/10.1016/j.enpol.2021.112703.

[4] Mohandes B, Moursi MSE, Hatziargyriou N, Khatib SE. A Review of Power System Flexibility With High Penetration of Renewables. IEEE Trans Power Syst 2019;34:3140–55. https://doi.org/10.1109/TPWRS.2019.2897727.

[5] Jin X, Wu Q, Jia H. Local flexibility markets: Literature review on concepts, models and clearing methods. Appl Energy 2020;261:114387. https://doi.org/https://doi.org/10.1016/j.apenergy.2019.114387.

[6] Correa-Florez CA, Michiorri A, Kariniotakis G. Optimal Participation of Residential Aggregators in Energy and Local Flexibility Markets. IEEE Trans Smart Grid 2020;11:1644–56. https://doi.org/10.1109/TSG.2019.2941687.

[7] Thorvaldsen KE, Korpås M, Farahmand H. Long-term Value of Flexibility from Flexible Assets in Building Operation. Int J Electr Power Energy Syst 2022;138:107811. https://doi.org/https://doi.org/10.1016/j.ijepes.2021.107811.

[8] Luo Z, Peng J, Cao J, Yin R, Zou B, Tan Y, et al. Demand Flexibility of Residential Buildings: Definitions, Flexible Loads, and Quantification Methods. Engineering 2022;16:123–40. https://doi.org/https://doi.org/10.1016/j.eng.2022.01.010.

[9] Jiang T, Li Z, Jin X, Chen H, Li X, Mu Y. Flexible operation of active distribution network using integrated smart buildings with heating, ventilation and air-conditioning systems. Appl Energy 2018;226:181–96. https://doi.org/https://doi.org/10.1016/j.apenergy.2018.05.091.

[10] Kanakadhurga D, Prabaharan N. Demand side management in microgrid: A critical review of key issues and recent trends. Renew Sustain Energy Rev 2022;156:111915. https://doi.org/https://doi.org/10.1016/j.rser.2021.111915.

[11] Sang L, Hu Q, Xu Y, Wu Z. Privacy-preserving Hybrid Cloud Framework for Real-time TCL-based Demand Response. IEEE Trans Cloud Comput 2022:1. https://doi.org/10.1109/TCC.2022.3142009.

[12] Tang H, Wang S, Li H. Flexibility categorization, sources, capabilities and technologies for energy-flexible and grid-responsive buildings: State-of-the-art and future perspective. Energy 2021;219:119598. https://doi.org/https://doi.org/10.1016/j.energy.2020.119598.

[13] Chen H, Wang D, Zhang R, Jiang T, Li X. Optimal participation of ADN in energy and reserve markets considering TSO-DSO interface and DERs uncertainties. Appl Energy 2022;308:118319. https://doi.org/https://doi.org/10.1016/j.apenergy.2021.118319.

[14] Pearson S, Wellnitz S, Crespo del Granado P, Hashemipour N. The value of TSO-DSO coordination in re-dispatch with flexible decentralized energy sources: Insights for Germany in 2030. Appl Energy 2022;326:119905. https://doi.org/https://doi.org/10.1016/j.apenergy.2022.119905.

[15] Edmunds C, Galloway S, Elders I, Bukhsh W, Telford R. Design of a DSO-TSO balancing market coordination scheme for decentralised energy. IET Gener Transm Distrib 2020;14:707–18. https://doi.org/https://doi.org/10.1049/iet-gtd.2019.0865.

[16] Vijay R, Mathuria P. Feasibility and flexibility regions estimation at TSO–DSO interconnection node using grid structure optimization. Sustain Energy, Grids Networks 2022;32:100952. https://doi.org/https://doi.org/10.1016/j.segan.2022.100952.

[17] Zhong C, Zhou Y, Chen J, Liu Z. DC-side synchronous active power control of two-stage photovoltaic generation for frequency support in Islanded microgrids. Energy Reports 2022;8:8361–71. https://doi.org/https://doi.org/10.1016/j.egyr.2022.06.030.

[18] Zhang S, Zhou Z, Luo R, Zhao R, Xiao Y, Xu Y. A low-carbon, fixed-tour scheduling problem with time windows in a time-dependent traffic environment. Int J Prod Res 2022:1–20. https://doi.org/10.1080/00207543.2022.2153940.

[19] Zou W, Sun Y, Zhou Y, Lu Q, Nie Y, Sun T, et al. Limited Sensing and Deep Data Mining: A New Exploration of Developing City-Wide Parking Guidance Systems. IEEE Intell Transp Syst Mag 2022;14:198–215. https://doi.org/10.1109/MITS.2020.2970185.

[20] Han Y, Wang B, Guan T, Tian D, Yang G, Wei W, et al. Research on Road Environmental Sense Method of Intelligent Vehicle Based on Tracking Check. IEEE Trans Intell Transp Syst 2023;24:1261–75. https://doi.org/10.1109/TITS.2022.3183893.

[21] Fang Y, Min H, Wu X, Wang W, Zhao X, Mao G. On-Ramp Merging Strategies of Connected and Automated Vehicles Considering Communication Delay. IEEE Trans Intell Transp Syst 2022;23:15298–312. https://doi.org/10.1109/TITS.2022.3140219.

[22] Borozan D. Asymmetric effects of policy uncertainty on renewable energy consumption in G7 countries. Renew Energy 2022;189:412–20. https://doi.org/https://doi.org/10.1016/j.renene.2022.02.055.

[23] Bagheri A, Jadid S. An IGDT-based multi-criteria TSO-DSO coordination scheme for simultaneously clearing wholesale and retail electricity auctions. Sustain Energy, Grids Networks 2022;32:100942. https://doi.org/https://doi.org/10.1016/j.segan.2022.100942.

[24] Kalantar-Neyestanaki M, Cherkaoui R. Risk-Aware Active Power Flexibility Allocation From TSO–DSO Interconnections: Switzerland's Transmission Network. IEEE Syst J 2022;16:6513–23. https://doi.org/10.1109/JSYST.2022.3164987.

[25] Ansaripour R, Barati H, Ghasemi A. A chance-constrained optimization framework for

transmission congestion management and frequency regulation in the presence of wind farms and energy storage systems. Electr Power Syst Res 2022;213:108712. https://doi.org/https://doi.org/10.1016/j.epsr.2022.108712.

[26] Hu M, Xiao F, Wang S. Neighborhood-level coordination and negotiation techniques for managing demand-side flexibility in residential microgrids. Renew Sustain Energy Rev 2021;135:110248. https://doi.org/https://doi.org/10.1016/j.rser.2020.110248.

[27] Rasheed MB, R-Moreno MD. Minimizing pricing policies based on user load profiles and residential demand responses in smart grids. Appl Energy 2022;310:118492. https://doi.org/https://doi.org/10.1016/j.apenergy.2021.118492.

[28] Amin A, Kem O, Gallegos P, Chervet P, Ksontini F, Mourshed M. Demand response in buildings: Unlocking energy flexibility through district-level electro-thermal simulation. Appl Energy 2022;305:117836. https://doi.org/https://doi.org/10.1016/j.apenergy.2021.117836.

[29] Khajeh H, Firoozi H, Laaksonen H. Flexibility Potential of a Smart Home to Provide TSO-DSO-level Services. Electr Power Syst Res 2022;205:107767. https://doi.org/https://doi.org/10.1016/j.epsr.2021.107767.

[30] Mansouri SA, Ahmarinejad A, Javadi MS, Nezhad AE, Shafie-Khah M, Catalão JPS. Demand response role for enhancing the flexibility of local energy systems. In: Graditi G, Di Somma MBT-DER in LIES, editors. Distrib. Energy Resour. Local Integr. Energy Syst. Optim. Oper. Plan., Elsevier; 2021, p. 279–313. https://doi.org/10.1016/B978-0-12-823899-8.00011-X.

[31] Gasca MV, Ibáñez F, Pozo D. Flexibility quantification of thermostatically controlled loads for demand response applications. Electr Power Syst Res 2022;202:107592. https://doi.org/https://doi.org/10.1016/j.epsr.2021.107592.

[32] Phani Raghav L, Seshu Kumar R, Koteswara Raju D, Singh AR. Analytic Hierarchy Process (AHP) – Swarm intelligence based flexible demand response management of grid-connected microgrid. Appl Energy 2022;306:118058.

https://doi.org/https://doi.org/10.1016/j.apenergy.2021.118058.

[33] Lai C-M, Teh J. Comprehensive review of the dynamic thermal rating system for sustainable electrical power systems. Energy Reports 2022;8:3263–88. https://doi.org/https://doi.org/10.1016/j.egyr.2022.02.085.

[34] Lai C-M, Teh J. Network topology optimisation based on dynamic thermal rating and battery storage systems for improved wind penetration and reliability. Appl Energy 2022;305:117837. https://doi.org/https://doi.org/10.1016/j.apenergy.2021.117837.

[35] Teh J, Lai C-M. Reliability impacts of the dynamic thermal rating and battery energy storage systems on wind-integrated power networks. Sustain Energy, Grids Networks 2019;20:100268. https://doi.org/https://doi.org/10.1016/j.segan.2019.100268.

[36] Metwaly MK, Teh J. Probabilistic Peak Demand Matching by Battery Energy Storage Alongside Dynamic Thermal Ratings and Demand Response for Enhanced Network Reliability. IEEE Access 2020;8:181547–59. https://doi.org/10.1109/ACCESS.2020.3024846.

[37] Setlhaolo D, Sichilalu S, Zhang J. Residential load management in an energy hub with heat pump water heater. Appl Energy 2017;208:551–60. https://doi.org/10.1016/j.apenergy.2017.09.099.

[38] Hou X, Wang J, Huang T, Wang T, Wang P. Smart Home Energy Management Optimization Method Considering Energy Storage and Electric Vehicle. IEEE Access 2019;7:144010–20. https://doi.org/10.1109/ACCESS.2019.2944878.

[39] Yuan H, Li F, Wei Y, Zhu J. Novel linearized power flow and linearized OPF models for active distribution networks with application in distribution LMP. IEEE Trans Smart Grid 2018;9:438–48. https://doi.org/10.1109/TSG.2016.2594814.

[40] Zhang C, Xu Y, Dong ZY. Robustly Coordinated Operation of a Multi-Energy Micro-Grid in Grid-Connected and Islanded Modes Under Uncertainties. IEEE Trans Sustain Energy 2020;11:640–51. https://doi.org/10.1109/TSTE.2019.2900082.

[41] Jiang T, Wu C, Zhang R, Li X, Chen H, Li G. Flexibility Clearing in Joint Energy and Flexibility

Markets Considering TSO-DSO Coordination. IEEE Trans Smart Grid 2022:1. https://doi.org/10.1109/TSG.2022.3153634.

[42] Steriotis K, Makris P, Tsaousoglou G, Efthymiopoulos N, Varvarigos E. Co-Optimization of Distributed Renewable Energy and Storage Investment Decisions in a TSO-DSO Coordination Framework. IEEE Trans Power Syst 2022:1–14. https://doi.org/10.1109/TPWRS.2022.3212919.

[43] Chen H, Fu L, Zhang R, Lin C, Jiang T, Li X, et al. Local energy market clearing of integrated ADN and district heating network coordinated with transmission system. Int J Electr Power Energy Syst 2021;125:106522. https://doi.org/https://doi.org/10.1016/j.ijepes.2020.106522.

[44] Wang B, Zhang C, Dong ZY. Interval Optimization Based Coordination of Demand Response and Battery Energy Storage System Considering SOC Management in a Microgrid. IEEE Trans Sustain Energy 2020;11:2922–31. https://doi.org/10.1109/TSTE.2020.2982205.